TIME-DOMAIN EQUALIZATION FOR UNDERWATER ACOUSTIC OFDM SYSTEMS WITH INSUFFICIENT CYCLIC PREFIX

KELVIN YEO SOON KEAT

B.Eng.(Hons.), NUS

A THESIS SUBMITTED FOR THE DEGREE OF MASTER OF ENGINEERING

DEPARTMENT OF ELECTRICAL AND COMPUTER ENGINEERING

2011

Acknowledgements

The author would like to thank his supervisors Professor Lawrence Wong and Dr Mandar Chitre for their invaluable guidance and support throughout the course of his academic pursuit. He would also like to thank Dr Konstantinos Pelekanakis for his patience, support and great insight in making this thesis possible.

Great thanks to all the friends and colleagues in ARL.

The author would also wish to express his greatest gratitude towards his family who has been enormously supportive.

Contents

Contents ii

List of Figures v

List of Tables viii

Nomenclature x

1 Introduction 1

1.1 Background 1

1.2 Literature review 2

1.3 Thesis Contribution 5

1.4 Thesis Outline 5

2 Orthogonal Frequency-Division Multiplexing 6

3 Time Domain Minimum Mean Square Error Channel Shortening Equalizers 11

3.1 Introduction 11

3.2 Minimum Mean Square Error Unit Tap Constraint 16

3.3 Minimum Mean Square Error Unit Energy Constraint 18
3.4 Comparison Between The Two Methods 19
3.5 Simulation Results 21

4 Time Domain Maximum Shortening Signal-to-Noise Ratio Channel Shortening Equalizers 28
4.1 MSSNR 28
4.2 Generic MSSNR 33
4.3 Minimum ISI 35
4.4 Simulation Results 38

5 Frequency Domain Decision Feedback Equalizer 43
5.1 Simulation Results 47

6 Trial Data 49
6.1 GLINT 08 51
6.1.1 Signal 1 52
6.1.2 Signal 2 57
6.2 Singapore Water 2010 64

7 Conclusion 71
7.1 Future Work 72

References 73

Summary

Orthogonal frequency division-multplexing (OFDM) is an effective method to tackle inter-symbol interference (ISI) in underwater acoustic communication and achieve high bit-rates. OFDM requires the length of the cyclic prefix (CP) to be as long as the channel length. However, in short-range shallow water or medium-range deep water acoustic links, the channels are as long as a few hundred taps. This reduces the bandwidth efficiency of the system. This thesis explores methods of reducing the length of CP in OFDM systems, and hence increasing the bandwidth efficiency of these systems. The role of a time domain CSE is to shorten the effective channel so that a shorter CP can be used. These methods include two time domain channel shortening equalizers (CSE): minimum mean square error (MMSE) and maximum shortening signal-to-noise ratio (MSSNR). Two of the more common MMSE CSEs are unit tap constraint (UTC) and unit energy constraint (UEC). The MSSNR approach and its frequency weighted model minimum ISI (Min ISI) are designed to minimize the shortening signal-to-noise ratio (SSNR). Another method to increase the bandwidth efficiency is by implementing the frequency domain decision feedback equalizer (FD-DFE). The performance of the different methods is evaluated on simulated and real acoustic data.

List of Figures

2.1 Cyclic Prefix inserted at the front of an OFDM symbol in time domain 7

2.2 OFDM systems with different CP. 8

2.3 Channel Shortening Equalizer on OFDM 10

3.1 MMSE Channel Shortening Equalizer 11

3.2 Effective impulse response. 21

3.3 SSNR plots for different Nb values. 22

3.4 SSNR plots for different filter lengths. 23

3.5 UEC SSNR against relative delay. 24

3.6 UTC SSNR against relative delay. 24

3.7 BER against SNR. 25

3.8 Frequency Responses and BER by sub-carriers. 26

3.9 BER against Eb/No. 27

4.1 BER against SNR plot. 38

4.2 SSNR against Relative Delay. 39

4.3 BER against EbNo plot 40

4.4 Colored Noise PSD 41

4.5 BER performance of equalizers in colored noise. 42

5.1 FD-DFE on OFDM 43
5.2 BER against SNR. 48
5.3 BER against EbNo 48

6.1 Processing of the received data 50
6.2 Motion of the transmitter with respect to a fixed receiver array (arbitrary coordinate system) 51
6.3 Spectrogram of received signal at D 52
6.4 Snapshots of the estimated time-varying channel impulse response for GLINT 08 Signal 1. The horizontal axis represents delay, the vertical axis represents absolute time and the colorbar represents the amplitude. The intensity ranges linearly. 53
6.5 Learning Curve for Signal 1 54
6.6 Effective CIR and original CIR of GLINT 08 signal 1. 55
6.7 Carrier Phase Estimate for Signal 1 56
6.8 PSD of Noise for GLINT 08 58
6.9 Frequency Response of TIR UEC and UTC for Signal 1 59
6.10 Snapshots of the estimated time-varying channel impulse response for GLINT 08 Signal 2. The horizontal axis represents delay, the vertical axis represents absolute time and the colorbar represents the amplitude. The intensity ranges linearly. 60
6.11 Learning Curve for Signal 2 61
6.12 Effective CIR and original CIR of GLINT 08 signal 2. 61
6.13 Carrier Phase Estimate for Signal 2 62

6.14 Frequency Response of TIR UEC and UTC for Signal 2 64
6.15 Snapshots of the estimated time-varying channel impulse response for Singapore Water 2010. The horizontal axis represents delay, the vertical axis represents absolute time and the colorbar represents the amplitude. The intensity ranges linearly. 65
6.16 Effective CIR and original CIR of Singapore Water 2010. 66
6.17 Carrier Phase Estimate for Singapore Water 2010 66
6.18 BER for Singapore Water 2010 68
6.19 PSD of Noise for Singapore Water 2010 69
6.20 Frequency Response of TIR UEC and UTC for Singapore Water 2010 70

List of Tables

6.1 OFDM Parameters of Signal 1 54
6.2 BER performance in Signal 1 57
6.3 OFDM Parameters of Signal 2 59
6.4 BER performance of Signal 2 62
6.5 OFDM Parameters of Singapore Water 2010 64
6.6 BER performance in Singapore Water 2010 67

List of Abbreviations

ARL Acoustic Research Lab Singapore

BER Bit Error Rate

CIR Channel Impulse Response

CP Cyclic Prefix

CSE Channel Shortening Equalizer

FD-DFE Frequency Domain Decision Feedback Equalizer

FFT Fast Fourier Transform

ICI Inter-Carrier Interference

IPAPA Improved Proportionate Affine Projection algorithm

IPNLMS Improved Proportionate Normalized Least Mean Square

ISI Inter-Symbol Interference

MMSE Minimum Mean Square Error

MSSNR Maximum Shortening Signal to Noise Ratio

NLMS Normalized Least Mean Square

OFDM Orthogonal Frequency Division-Multplexing

RLS Recursive Least Square

SNR Signal to Noise Ratio

SSNR Shortening Signal to Noise Ratio

TIR Target Impulse Response

UEC Unit Energy Constraint

UTC Unit Tap Constraint

UWA Underwater Acoustic

Chapter 1

Introduction

1.1 Background

Underwater communications have been given much attention by scientists and engineers alike because of their application in marine research, oceanography, marine commercial operations, the offshore oil industry and defense. Sound propagation proves to be most popular because electromagnetic as well as optical waves attenuate rapidly underwater.

For the past 30 years, much progress has been made in the field of underwater acoustic (UWA) communication [1]. However, due to the unique channel characteristics like fading, extended multipath and the refractive properties of a sound channel [2], UWA communication is not without its challenges. One of the issues a designer for the communication system of a wide-band UWA channel faces is the time varying and long impulse response. In medium range (200m to 2km) very shallow (50m to 200m) water channels, which are common in coastal regions like Singapore waters, long impulse responses due to extended multipath are more

severe. Long impulse response contributes to inter-symbol interference (ISI) and is an undesirable channel characteristic because of its negative impact on the error rate. In recent years, much work has been done on implementing orthogonal frequency-division multiplexing (OFDM) for UWA communication [3; 4]. When the cyclic prefix (CP) is longer than the channel impulse response (CIR), OFDM is an effective method to tackle ISI and has yielded good results in UWA channels. However, long CP is not desirable because it will reduce the bandwidth efficiency of the system. Bandwidth efficiency, a measure of the channel throughput, can be computed by $\frac{N_c}{N_c+N_p}$ where N_c is the number of sub-carriers and N_p is the CP length. Hence, to keep the bandwidth efficiency high, it is important that the CP is as short as possible. A time domain equalizer, known as a channel shortening equalizer (CSE), can be inserted before the OFDM demodulator to shorten the effective channel so that a smaller N_p is required. A channel shortening equalizer (CSE) is also known as a partial response equalizer. A CSE has better channel shortening capability then a full response equalizer in general because a CSE does not impose any limitation on the shape of the effective impulse response. The output SNR of a CSE is higher than the output SNR of a full equalizer.

1.2 Literature review

Large delay spread is one of the challenges of underwater communication that scientists and engineers try to overcome. Some work has been done in implementing decision feedback equalizer (DFE) on underwater communication systems [5]. However, DFEs for channels with large delay spread require high computational power due to the long feedback filters. In [6; 7; 8], the authors have implemented

modified DFEs, which factor in the length and the sparsity of the channel. Another method to counter the effect of large delay spread in underwater acoustic channels is the turbo equalizer [9]. Turbo equalizer, however, requires high computation power. Two methods that are most commonly used to overcome the large delay spread in underwater acoustic OFDM systems are: CSE and frequency domain equalizer.

Over the years, scientists have made tremendous progress in developing and applying CSE in different areas. [10; 11; 12; 13; 14; 15].The idea of CSEs first came about in the 1970s [10; 11]. In [11], the effective CIR at the output of the equalizer, also known as the target impulse response (TIR), is a truncated form of the original impulse response. Dhahir and Chow proposed a minimum mean square error (MMSE) CSE that minimizes the mean square error (MSE) between the equalizer output and the TIR output [12; 13]. The CSE was first developed to work with maximum-likelihood sequence estimation (MLSE) to achieve higher data rates on bandlimited noisy linear channels. The role of the CSE is to reduce the CIR to allow practical use of the high performance Viterbi algorithm. In order to avoid a trivial solution, some constraints like unit energy constraint (UEC) and unit tap constraint (UTC) has be imposed on the TIR. In maximum shortening signal-to-noise ratio (MSSNR), the finite impulse response (FIR) filter is generated to minimize the energy outside the length of a TIR while setting the unit energy constraint on the desired component of the received signal [15]. Using Cholesky decomposition, the vector that solves for the generalized Rayleigh Quotient gives the equalizer taps. The drawback of this method is that the filter length has to be shorter than the TIR length in order to keep the matrix for Cholesky decomposition positive semi-definite. In a long delay spread scenario,

we wish to have a sufficiently long filter and a short TIR. In [16], a new method of deriving the matrix for MSSNR is shown to eliminate the restriction on the filter length. The MSSNR proposed in [15] is a zero forcing equalizer where noise is ignored. A more general derivation of MSSNR that takes into account the statistic of the noise is proposed in [17]. However, the method is not optimized for sub-carrier SNR. The minimum ISI (Min ISI) is a frequency weighted form of MSSNR [18; 19]. It minimizes the energy outside the length of the TIR according to the sub-carrier SNR. By using a water pouring algorithm the objective function in sub-carriers with higher SNR is amplified. Both MSSNR and Min ISI have been implemented in the Assymetrical Digital Subscriber Loop (ADSL) system to increase bandwidth efficiency. Other CSEs that involve frequency weighting are covered in [20; 21; 22]. The authors in [23] and [24] show the performance of MSSNR and MMSE, respectively, in OFDM with insufficient CP. In [25], the authors compare the performance of MMSE UEC and MSSNR in UWA OFDM systems. However, due to limitation on the filter length of MSSNR as stated in [15], and to have a fair comparison, both of the CSEs have filter length shorter than the CP length.

An alternative to time domain equalizers is their frequency domain counterparts. Frequency domain equalizer for OFDM with insufficient CP are covered in [26; 27; 28]. Among the frequency domain equalizers covered, frequency domain DFE gives the best bit error result [27].

1.3 Thesis Contribution

The objective of this thesis is to study methods to increase the bandwidth efficiency of an OFDM communication system in an UWA channel by decreasing the CP length. The study of the different equalizers is performed on an OFDM platform to keep in line with the objective of the thesis. The main contributions of this thesis are:

i. Provide a more detailed mathematical derivation of different CSEs and FDDFE.

ii. Compare the BER performance of different CSEs and FDDFE on simulated and actual UWA trial data.

iii. Demonstrate a receiver structure that includes a CSE and a sparse channel estimator.

1.4 Thesis Outline

This thesis is organized in 7 chapters. Chapter 1 is dedicated to provide the background knowledge on UWA communications and the thesis objective. In Chapter 2, a brief description of OFDM is provided to have a better appreciation of the role of CSE. Chapter 3-5 cover the theoretical framework of various CSEs with description of the parameters of the simulation and some simulation results. Chapter 6 shows the analysis of the performance of different CSEs on real UWA data. Lastly, Chapter 7 sums up the thesis and propose further work to build on the current research.

Chapter 2

Orthogonal Frequency-Division Multiplexing

OFDM is a communication technique which divides the available bandwidth into several sub-carriers [29]. Each sub-carrier is allocated a narrow band which is less than the coherence bandwidth of the channel such that the sub-carriers experience flat fading. The symbols in each sub-carrier can be modulated using any modulation scheme. OFDM is implemented by using the Inverse Discrete Fourier Transform (IDFT) and DFT to map symbols in frequency domain to signals in time domain and vice-versa. An OFDM system eliminates ISI due to multipath arrival by introducing a guard interval between adjacent OFDM symbols. If the guard interval is larger than the delay spread of the channel, ISI is completely eliminated. The guard interval is usually introduced in the form of a CP or zero padding. An OFDM symbol is orthogonal as long as delay spread is shorter than the CP.

For channels with large delay spread, like the short to medium range shallow

UWA channels, OFDM systems have low bandwidth efficiency. The CP in an OFDM system does not carry any data. The longer the CP is, the more redundancy is introduced to the system. For a practical signal bandwidth, the delay spread of a UWA channel can span up to hundreds of symbols. Besides, due to high Doppler frequency, there is a limitation to the number of sub-carriers we can use for OFDM in UWA channels [30].

Besides, long CP leads to long symbol duration, which is not desirable when the channel coherence time is short. In UWA communication channels the coherence time is short due to displacement of the reflection point for the signal induced by the surface waves [31].

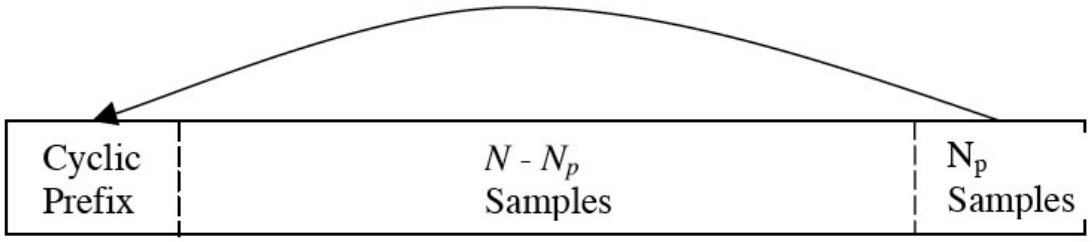

Figure 2.1: Cyclic Prefix inserted at the front of an OFDM symbol in time domain

Figure 2.1 shows an OFDM symbol with CP. The CP is simply the last N_p samples of the OFDM symbol in time domain. It is inserted at the start of the OFDM symbol. The CP length affects the bandwidth efficiency of an OFDM system. Figure 2.2 shows the scenario of two OFDM symbols with different CP length. The number of sub-carriers N_c is the same for both symbol. Both symbols carry the same number of data. However, the one with longer symbol duration has lower efficiency because CP does not carry data bits. Bandwidth efficiency of an OFDM system is given by $\frac{N_c}{N_c+N_p}$.

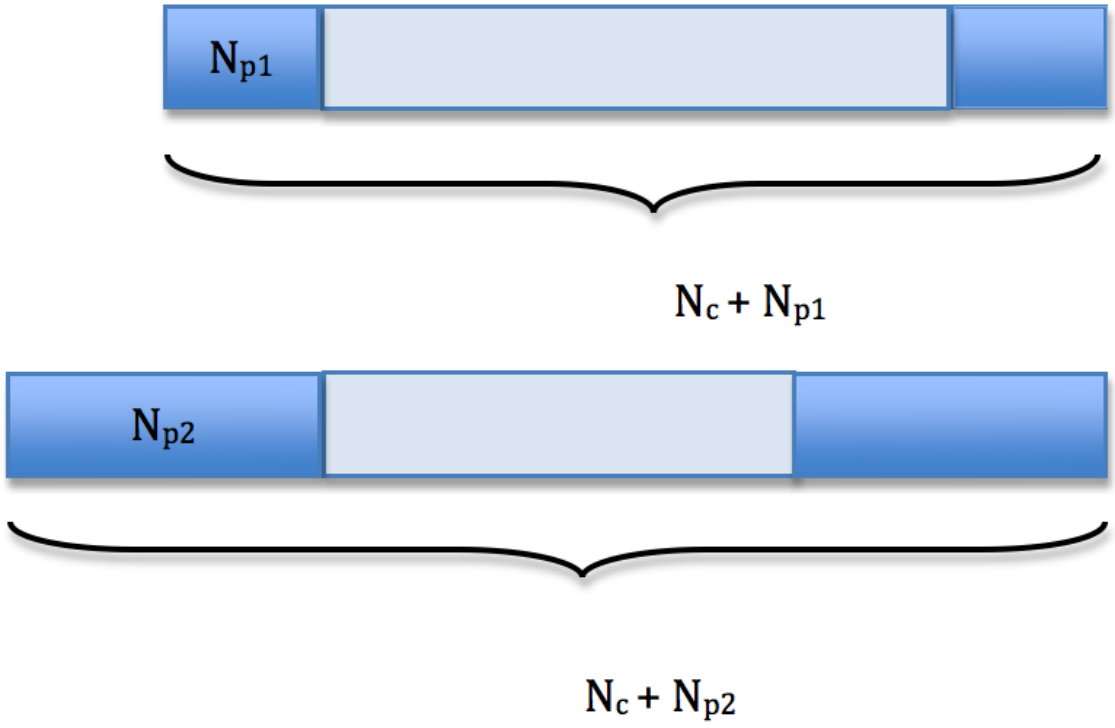

Figure 2.2: OFDM systems with different CP.

Let $\mathbf{X}$ be the PSK modulated data symbols.

$$\mathbf{x}_i = \mathbf{Q}^H \mathbf{X}_i \tag{2.1}$$

where $\mathbf{x}_i$ are the time domain samples in the current OFDM symbol and $\mathbf{Q}$ is the discrete Fourier matrix. The index i represents the OFDM symbol index and n is the time index within the OFDM symbol in time domain. The received sequence $\tilde{y}_i(n)$ is:

$$\tilde{y}_i(n) = \sum_{l=0}^{L} \tilde{x}_i(n-l)h_l + z_n \tag{2.2}$$

where $_l$ and z_n are the channel impulse respones and the noise sequence respectively. Let $\mathbf{y}_i$ be the received sequence with CP removed.

$$\begin{aligned} \mathbf{y}_i &= \begin{bmatrix} h_0 & 0 & . & 0 & h_L & h_{L-1} & . & h_1 \\ h_1 & h_0 & 0 & . & 0 & h_L & . & h_2 \\ \vdots & & & & & & & \\ 0 & . & 0 & h_L & h_{L-1} & . & h_1 & h_0 \end{bmatrix} \mathbf{x}_i + \mathbf{z} \\ &= \mathbf{H}\mathbf{x}_i + \mathbf{z} \end{aligned} \tag{2.3}$$

where $\mathbf{z}$ is the noise sequence. Because of CP, $\mathbf{H}$ is a circulant matrix. According to matrix theory [32], a N_cxN_c circulant matrix can be decomposed into:

$$\mathbf{H} = \mathbf{Q}^H \mathbf{\Lambda} \mathbf{Q} \tag{2.4}$$

where $\mathbf{\Lambda}$ is a diagonal matrix whose elements are the FFT of the zero padded channel impulse response. To recover the PSK modulated symbols from the

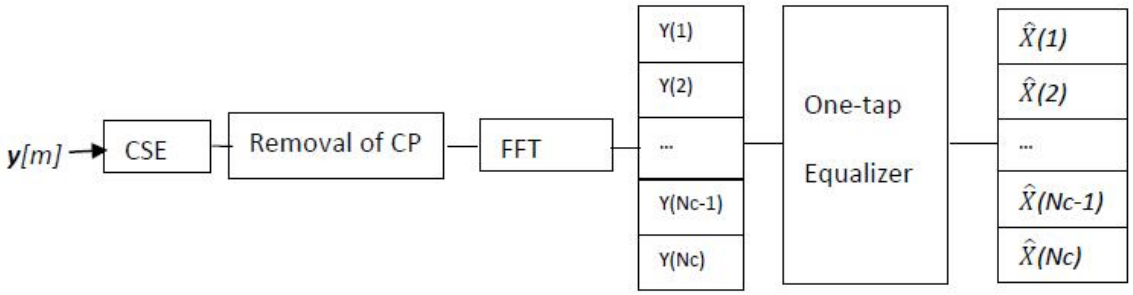

Figure 2.3: Channel Shortening Equalizer on OFDM

received sequence,

$$\begin{aligned} \mathbf{Y}_i &= \mathbf{Q}\mathbf{y}_i \\ &= \mathbf{Q}\mathbf{Q}^H\mathbf{\Lambda}\mathbf{Q}\mathbf{Q}^H\mathbf{X}_i + \mathbf{Z} \\ &= \mathbf{\Lambda}\mathbf{X}_i + \mathbf{Z} \end{aligned} \tag{2.5}$$

This is valid as long as the CIR is time invariant within the symbol duration. As shown, only a 1-tap equalizer is needed to recover the transmitted data symbol from the received sequence.

The long CIR is a common feature in shallow medium range UWA communication. To shorten the CIR, a time domain CSE can be applied before the FFT operation to shorten the channel. Figure 2.3 shows the application of CSE on OFDM. The 1-tap equalizer is generated based on the effective impulse response which is the convolution of the CIR and the TIR.

Chapter 3

Time Domain Minimum Mean Square Error Channel Shortening Equalizers

3.1 Introduction

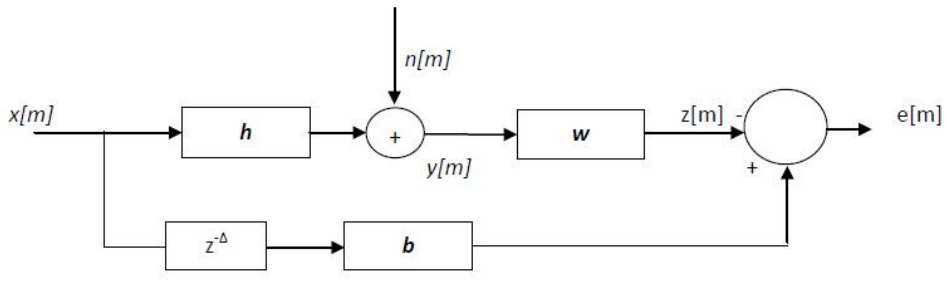

Figure 3.1: MMSE Channel Shortening Equalizer

The MMSE CSE is a class of equalizers that generates FIR filter that mini-

mizes the error between the output of the equalizer and the output of the TIR in the mean square sense. The TIR is shorter than the original CIR, and in an OFDM system, shorter than the CP. Figure 3.1 shows the block diagram of a MMSE CSE. The design problem for MMSE CSE is to compute the equalizer coefficients **w** and TIR **b** of a pre-defined length, such that the mean square of the error sequence is minimized. A certain constraint is imposed on the tir and based on this constraint the equalizer and TIR coefficients are calculated simultaneously. The vector $\boldsymbol{y}$[m] represents the received symbols. The CIR $\boldsymbol{h}$ has $l+1$ generally complex taps and is modeled as the combination of the effects of the transmitter filter, channel distortion and front-end receiver filter.

The equalizer $\boldsymbol{w}$ is a FIR filter with $N_f + 1$ taps. Across a block of $N_f + 1$ output symbols, the input-output relationship can be presented as follow:

$$\begin{bmatrix} y[m] \\ y[m-1] \\ . \\ . \\ . \\ y[m-N_f+1] \end{bmatrix} = \begin{bmatrix} h_0 & h_1 & \dots & h_l & 0 & \dots & 0 \\ 0 & h_0 & h_1 & \dots & h_l & 0 & \dots \\ . & & & & & & . \\ . & & & & & & . \\ . & & & & & & . \\ 0 & \dots & 0 & h_0 & h_1 & \dots & h_l \end{bmatrix} \times \begin{bmatrix} x[m] \\ x[m-1] \\ . \\ . \\ . \\ x[m-N_f+l] \end{bmatrix} + \begin{bmatrix} n[m] \\ n[m-1] \\ . \\ . \\ . \\ n[m-N_f+l] \end{bmatrix} \quad (3.1)$$

which is the same as the matrix form:

$$\mathbf{y}[m] = \mathbf{H}\mathbf{x}[m] + \mathbf{n}[m]. \tag{3.2}$$

For a system with oversampling factor bigger than one, the elements in $\mathbf{H}$ are vectors of length l_{os}, the oversampling factor. This becomes a fractionally spaced equalizer scenario. The input sequence $\{x[m]\}$ and the noise sequence $\{n[m]\}$ are assumed to be complex, have zero mean and are independent of each other. The input autocorrelation matrix, $\mathbf{R}_{xx}$ is defined by

$$\mathbf{R}_{xx} \equiv E[\mathbf{x}[m]\mathbf{x}[m]^H]$$

and the noise autocorreation matrix is,

$$\mathbf{R}_{nn} \equiv E[\mathbf{n}[m]\mathbf{n}[m]^H]$$

Both $\mathbf{R}_{xx}$ and $\mathbf{R}_{nn}$ are assumed to be positive-definite correlation matrices.The input-output cross-correlation and the output autocorrelation are defined as:

$$\mathbf{R}_{xy} \equiv E[\mathbf{x}[m]\mathbf{y}[m]^H] = \mathbf{R}_{xx}\mathbf{H}^H \tag{3.3}$$

$$\mathbf{R}_{yy} \equiv E[\mathbf{y}[m]\mathbf{y}[m]^H] = \mathbf{H}\mathbf{R}_{xx}\mathbf{H}^H + \mathbf{R}_{nn} \tag{3.4}$$

The objective is to compute the coefficients of the equalizer $\mathbf{w}$ given N_b the length of $\mathbf{b}$ such that the mean square of the error $e[m]$ is minimized.

The TIR $\mathbf{b}$ is not restricted to be causal. This allows one extra parameter to be introduced for better performance. A relative delay, Δ between the equalizer

and the TIR is assumed. Given:

$$s \equiv N_f + l - \Delta - N_b$$

the error $e[m]$ in Figure 3.1 can be expressed as

$$\begin{aligned} e[m] &= \sum_{j=0}^{N_b-1} {b_j}^* x[m-j-\Delta] - \sum_{k=0}^{N_f-1} {w_k}^* y[m-k] \qquad (3.5) \\ &= \begin{bmatrix} \mathbf{0}_{1\times\Delta} & b_0^* & b_1^* & \dots & b_{N_b-1}^* & \mathbf{0}_{1\times s} \end{bmatrix} \mathbf{x}[m] \\ &\quad - \begin{bmatrix} w_0^* & w_1^* & \dots & w_{N_f-1}^* \end{bmatrix} \mathbf{y}[m] \\ &\equiv \tilde{\mathbf{b}}^H \mathbf{x}[m] - \mathbf{w}^H \mathbf{y}[m] \qquad (3.6) \end{aligned}$$

Hence, the mean square error (MSE) is given by:

$$\begin{aligned} MSE &\equiv E[|e[m]|^2] \\ &= E[(\tilde{\mathbf{b}}^H \mathbf{x}[m] - \mathbf{w}^H \mathbf{y}[m])(\tilde{\mathbf{b}}^H \mathbf{x}[m] - \mathbf{w}^H \mathbf{y}[m])^H] \qquad (3.7) \\ &= \tilde{\mathbf{b}}^H \mathbf{R}_{xx} \tilde{\mathbf{b}} - \tilde{\mathbf{b}}^H \mathbf{R}_{xy} \mathbf{w} - \mathbf{w}^H \mathbf{R}_{yx} \tilde{\mathbf{b}} + \mathbf{w}^H \mathbf{R}_{yy} \mathbf{w}. \qquad (3.8) \end{aligned}$$

By applying the orthogonality principle which states that the error is uncorrelated with the observed data [33], we get:

$$\begin{aligned} E[e[m]\mathbf{y}[m]] &= \mathbf{0}_{1\times l} \\ \Rightarrow \tilde{\mathbf{b}}^H \mathbf{R}_{xy} &= \mathbf{w}^H \mathbf{R}_{yy} \qquad (3.9) \end{aligned}$$

Combining equations 3.8 and 3.9 we have:

$$MSE = \tilde{\mathbf{b}}^H \bar{\mathbf{R}}_{xy} \tilde{\mathbf{b}} \tag{3.10}$$

where

$$\begin{aligned} \bar{\mathbf{R}}_{xy} &= \mathbf{R}_{xx} - \mathbf{R}_{xy}\mathbf{R}_{yy}^{-1}\mathbf{R}_{yx} && (3.11)\\ &= \mathbf{R}_{xy} - \mathbf{R}_{xy}\mathbf{H}^H(\mathbf{H}\mathbf{R}_{xx}\mathbf{H}^H + \mathbf{R}_{nn})^{-1}\mathbf{H}\mathbf{R}_{xx} && (3.12)\\ &= [\mathbf{R}_{xx}^{-1} + \mathbf{H}^H\mathbf{R}_{nn}^{-1}\mathbf{H}]^{-1} && (3.13) \end{aligned}$$

by applying matrix inversion lemma and assuming $\mathbf{R}_{xx}$ and $\mathbf{R}_{nn}$ are invertible. We define a new matrix $\mathbf{R}_\Delta$:

$$\begin{aligned} \mathbf{R}_\Delta \equiv & \begin{bmatrix} \mathbf{0}_{N_b\times\Delta} & \mathbf{I}_{N_b} & \mathbf{0}_{N_b\times s} \end{bmatrix} \\ & .\bar{\mathbf{R}}_{xy} \begin{bmatrix} \mathbf{0}_{\Delta\times N_b} \\ \mathbf{I}_{N_b} \\ \mathbf{0}_{s\times N_b} \end{bmatrix} \end{aligned} \tag{3.14}$$

where $\mathbf{I}_{N_b}$ is an identity matrix of size N_b. Equation 3.9 becomes

$$\begin{aligned} MSE &= \begin{bmatrix} b_0^* & b_1^* & \dots & b_{N_b-1}^* \end{bmatrix} \mathbf{R}_\Delta \begin{bmatrix} b_0^* \\ b_1^* \\ \dots \\ b_{N_b-1}^* \end{bmatrix} \\ &\equiv \mathbf{b}^H\mathbf{R}_\Delta\mathbf{b} && (3.15) \end{aligned}$$

3.2 Minimum Mean Square Error Unit Tap Constraint

In order to avoid a trivial solution of $\mathbf{b} = \mathbf{w} = 0$, a constraint is placed on $\mathbf{b}$ [12]. For MMSE UTC, the MSE is minimized subject to $\mathbf{b}^H\mathbf{e}_i = 1$ where $\mathbf{e}_i$ is the ith unit vector. The Lagrangian for this optimization problem becomes:

$$L^{UTC}(\mathbf{b}, \lambda) = \mathbf{b}^H\mathbf{R}_\Delta\mathbf{b} + \lambda(\mathbf{b}^H\mathbf{e}_i - 1). \tag{3.16}$$

Setting $[dL^{UTC}(\mathbf{b}, \lambda)]/d\mathbf{b} = 0$, we have

$$2\mathbf{R}_\Delta\mathbf{b}_opt + \lambda\mathbf{e}_i = 0. \tag{3.17}$$

The optimal TIR coefficients are given by

$$\mathbf{b}_{opt} = \frac{\mathbf{R}_\Delta^{-1}\mathbf{e}_{i_{opt}}}{\mathbf{R}_\Delta^{-1}(i_{opt}, i_{opt})}. \tag{3.18}$$

where i_{opt} represents the index that yields the minimum mean-square error

$$MMSE^{UTC} = \frac{1}{\mathbf{R}_\Delta^{-1}(i_{opt}, i_{opt})} \tag{3.19}$$

and is derived from

$$i_{opt} = \arg\max_i \mathbf{R}_\Delta^{-1}(i, i). \tag{3.20}$$

where $\mathbf{R}_{\Delta}^{-1}(i,i)$ is the ith diagonal component of $\mathbf{R}_{\Delta}^{-1}$. Combining 3.9 and 3.18, the optimum equalizer coefficients are

$$\begin{aligned} \mathbf{w}_{opt}^{*} &= \tilde{\mathbf{b}}_{opt}^{H}\mathbf{R}_{xy}\mathbf{R}_{yy}^{-1} \\ &= \tilde{\mathbf{b}}_{opt}^{H}\mathbf{R}_{xx}\mathbf{H}^{H}(\mathbf{H}\mathbf{R}_{xx}\mathbf{H}+\mathbf{R}_{xx})^{-1} \end{aligned} \tag{3.21}$$

In [13], another method of deriving the equalizer coefficients based on UTC MMSE is introduced. It has some similarities with MMSE Decision Feedback Equalizer(DFE). However, it makes no assumption on the monicity and causality of the equalizer filter. Subject to UTC,$\mathbf{b}^{H}\mathbf{e}_i = 1$ and i is between 0 and $N_b - 1$, and equation 3.6 can be rewritten as follows:

$$e[m] = x[m-\Delta-i] - \mathbf{v}^{*}\mathbf{u} \tag{3.22}$$

where

$$\begin{aligned} \mathbf{v}^{*} &\equiv \begin{bmatrix} w_0^{*} & \dots & w_{N_f-1}^{*} & -b_0^{*} & \dots & -b_{i-1}^{*} & -b_{i+1}^{*} & \dots & -b_{N_b-1}^{*} \end{bmatrix} \\ \mathbf{u} &\equiv \begin{bmatrix} \mathbf{y}[m] \\ \mathbf{x}[m] \end{bmatrix} \end{aligned}$$

By applying standard Wiener [34] and solving for equalizer that gives the MMSE, we get:

$$\mathbf{v}_{opt}^{*} = \mathbf{R}_{x[m-\Delta-i]\mathbf{u}}\mathbf{R}_{\mathbf{uu}}^{-1} \tag{3.23}$$

The results in [12] shows that both methods yield the same output SNR. In the second method however, the search of the optimal i and Δ is exhaustive.The second method also limits the constraint to UTC whereas by having a Lagrangian term some other constraints can be used.

3.3 Minimum Mean Square Error Unit Energy Constraint

Another constraint on $\mathbf{b}$ is the UEC. This constraint has an advantage over UTC because the exhaustive search procedure for the optimal index i is no longer required. Under the constraint $\mathbf{b}^H\mathbf{b} = 1$, the Lagrangian in equation 3.16 is modified to

$$L^{UEC}(\mathbf{b}, \lambda) = \mathbf{b}^H\mathbf{R}_\Delta\mathbf{b} + \lambda(\mathbf{b}^H\mathbf{b} - 1). \tag{3.24}$$

By setting $[dL^{UEC}(\mathbf{b}, \lambda)]/d\mathbf{b} = 0$, we get

$$\mathbf{R}_\Delta\mathbf{b}_{opt} = \lambda\mathbf{b}_{opt} \tag{3.25}$$

The optimal TIR $\mathbf{b}_{opt}$ and λ is an eigenvector and eigenvalue of $\mathbf{R}_\Delta$, respectively. $\mathbf{R}_\Delta$ is a Hermitian positive-definite matrix. The MSE is given by

$$\begin{aligned} MSE &= \mathbf{b}_{opt}^H\mathbf{R}_\Delta\mathbf{b}_{opt} \\ &= \lambda\mathbf{b}_{opt}^H\mathbf{b}_{opt} \\ &= \lambda \end{aligned} \tag{3.26}$$

In order to minimize the MSE, $\mathbf{b}_{opt}$ is chosen to be the eigenvector that corresponds to the minimum eigenvalue, denoted by λ_{min} of $\mathbf{R}_{\Delta}$. The MMSE is equal to

$$MMSE^{UEC} = \lambda_{min}. \tag{3.27}$$

A more general model of UEC that allows weighting to emphasize some elements of the TIR is developed. We replace $\mathbf{b}^H\mathbf{b} = 1$ with $\mathbf{b}^H\mathbf{G}\mathbf{b} = 1$ where $\mathbf{G}$, a positive definite diagonal matrix, is the weighting matrix. Equation 3.25 becomes

$$\mathbf{R}_{\Delta}\mathbf{b}_{opt} = \lambda\mathbf{G}\mathbf{b}_{opt}. \tag{3.28}$$

In this case, $\mathbf{b}_{opt}$ is the generalized eigenvector of $\mathbf{R}_{\Delta}$ [35].

3.4 Comparison Between The Two Methods

The comparison between the UTC and UEC based MMSE CSE is made on the MMSE. We define the orthogonal eigen decomposition of $\mathbf{R}_{\Delta}$ as [35]:

$$\begin{aligned}
\mathbf{R}_{\Delta} &= \mathbf{U}\Lambda\mathbf{U}^H && (3.29)\\
\Rightarrow \mathbf{R}_{\Delta}^{-1} &= \mathbf{U}\Lambda^{-1}\mathbf{U}^H && (3.30)\\
\mathbf{R}_{\Delta}^{-1}(i,i) &= (\mathbf{e}_i^T\mathbf{U})\Lambda^{-1}(\mathbf{U}^H\mathbf{e}_i)\\
&\equiv \lambda_0^{-1}|u_{i,0}|^2 + \ldots + \lambda_{N_b}^{-1}|u_{i,N_b}|^2\\
&\leq \lambda_{min}^{-1} && (3.31)
\end{aligned}$$

In equation 3.31, $u_{i,j}$ denotes the (i, j) element of $\mathbf{U}$. Therefore

$$\begin{aligned} \Rightarrow MMSE^{UEC} &= \lambda_{min} \\ &\leq \frac{1}{\mathbf{R}_{\Delta}^{-1}(i,i)} \\ &= MMSE^{UTC} \end{aligned}$$

The equality only occurs when all of the eigenvalues of $\mathbf{R}_{\Delta}$ are equal.

Next we look at the shortening SNR (SSNR) which is the ratio of the signal power within the TIR length to signal outside the TIR lenght and noise. The SSNR can be defined as $|\mathbf{b}|^2/MMSE$[12]. To prove that SSNR of UEC is higher than UTC, we have to show that

$$\frac{MMSE^{UEC}}{|\mathbf{b}_{opt}^{UEC}|^2} \leq \frac{MMSE^{UTC}}{|\mathbf{b}_{opt}^{UTC}|^2} \tag{3.32}$$

By definition, $\mathbf{b}_{opt}^{UEC}$ gives the lowest MSE among all other unit norm TIR. It gives lower MSE than the choice $\mathbf{b}_{opt}^{UTC}/|\mathbf{b}_{opt}^{UTC}|$.Hence

$$\begin{aligned} \frac{MMSE^{UEC}}{|\mathbf{b}_{opt}^{UEC}|^2} &= MMSE^{UEC} \\ &\leq MSE_{|\mathbf{b}=\mathbf{b}_{opt}^{UTC}/|\mathbf{b}_{opt}^{UTC}|} \\ &\equiv \frac{MMSE^{UTC}}{|\mathbf{b}_{opt}^{UTC}|^2} \end{aligned} \tag{3.33}$$

which also proves that $MMSE^{UEC} \leq MMSE^{UEC}$ because $|\mathbf{b}_{opt}^{UTC}|^2 \geq 1$ without having to fix the delay for both constraints to be the same.

3.5 Simulation Results

The CIR used for the simulations is estimated from real acoustic data acquired in FAF 05 [1]. Figure 3.2 shows the effective impulse response of the output of

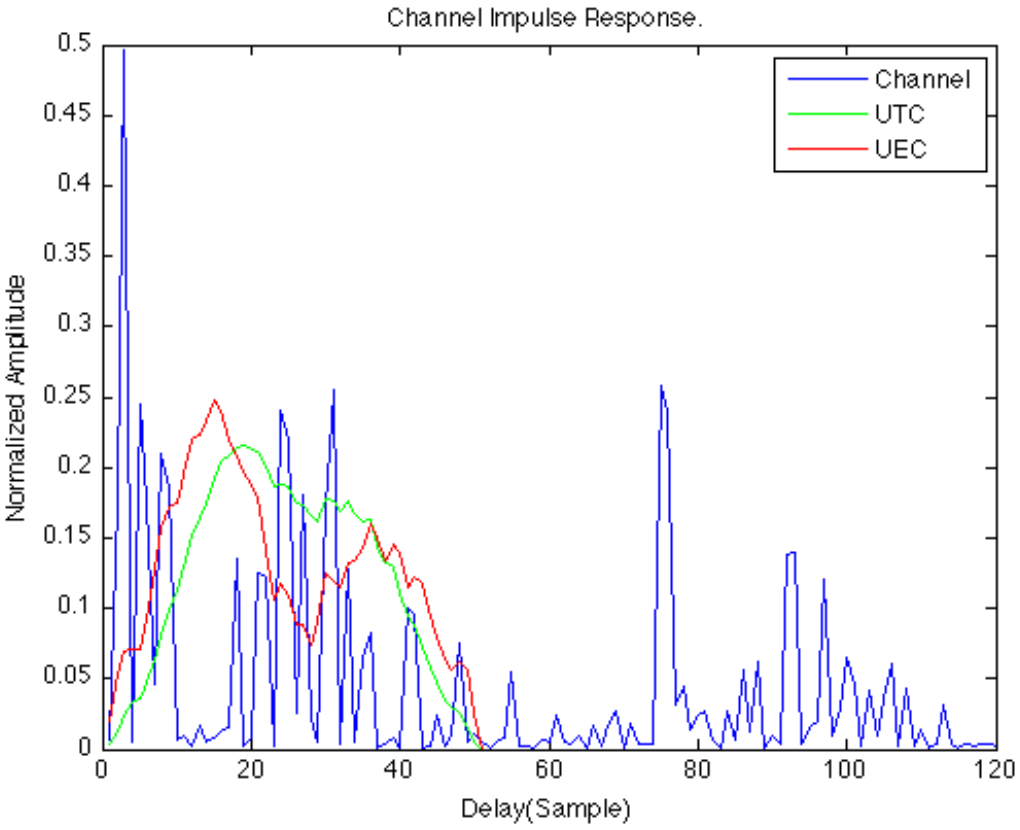

Figure 3.2: Effective impulse response.

the equalizer superimposed on the actual CIR. Notice that the effective impulse response is shorter than the actual CIR. The data used for the simulation is QPSK modulated in frequency domain. The CSEs, UTC and UEC, are inserted to shorten the CIR. The number of sub-carriers N_c is 512. The term N_b in the

[1]Focused Acoustic Forecasting 2005, July 2005 Pianosa Italy.

plots represent the length of the TIR which is also the CP length of the OFDM system. Figure 3.3 is the SSNR to the received signal SNR plot. As shown in equation 3.33, SSNR of UEC is higher than UTC when the filter lengths for both equalizers are fixed. As the TIR length increases, the SSNR of both UTC and

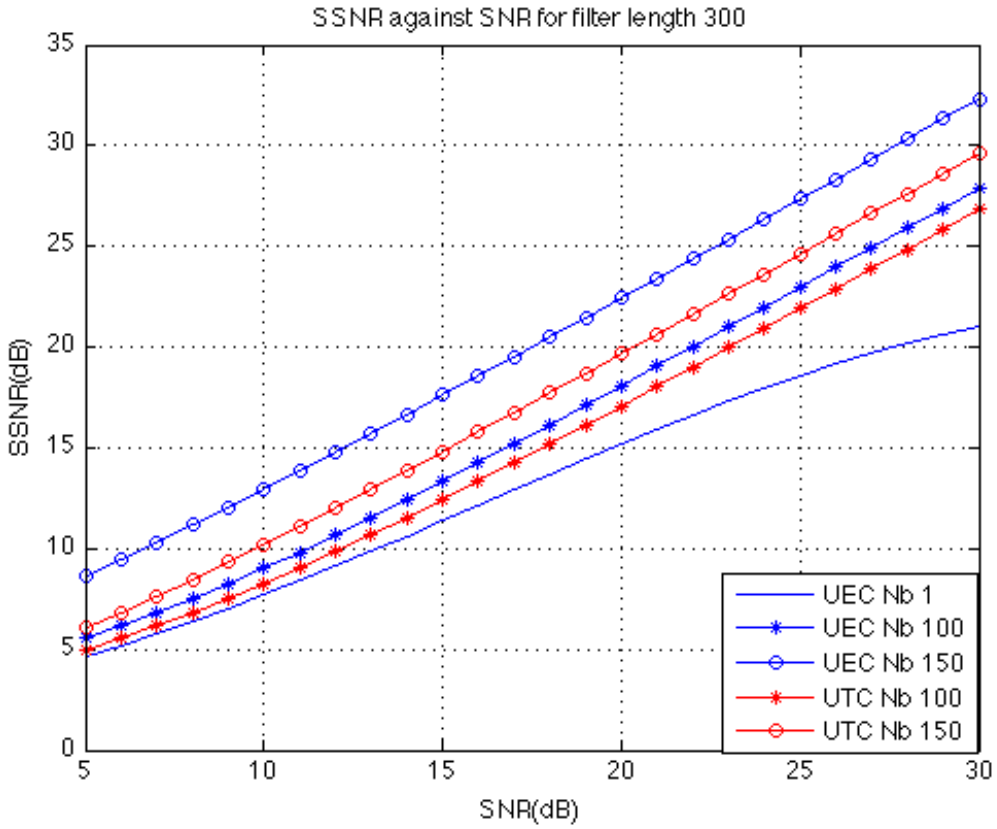

Figure 3.3: SSNR plots for different Nb values.

UEC increase. When N_b is one, the CSE becomes a linear MMSE equalizer. The SSNR plot shows a better performance by CSEs as compared to a linear MMSE equalizer.

Figure 3.4 is the SSNR to SNR plot of UEC and UTC with different filter length. The TIR length is set to 100 samples long. The SSNR of both systems

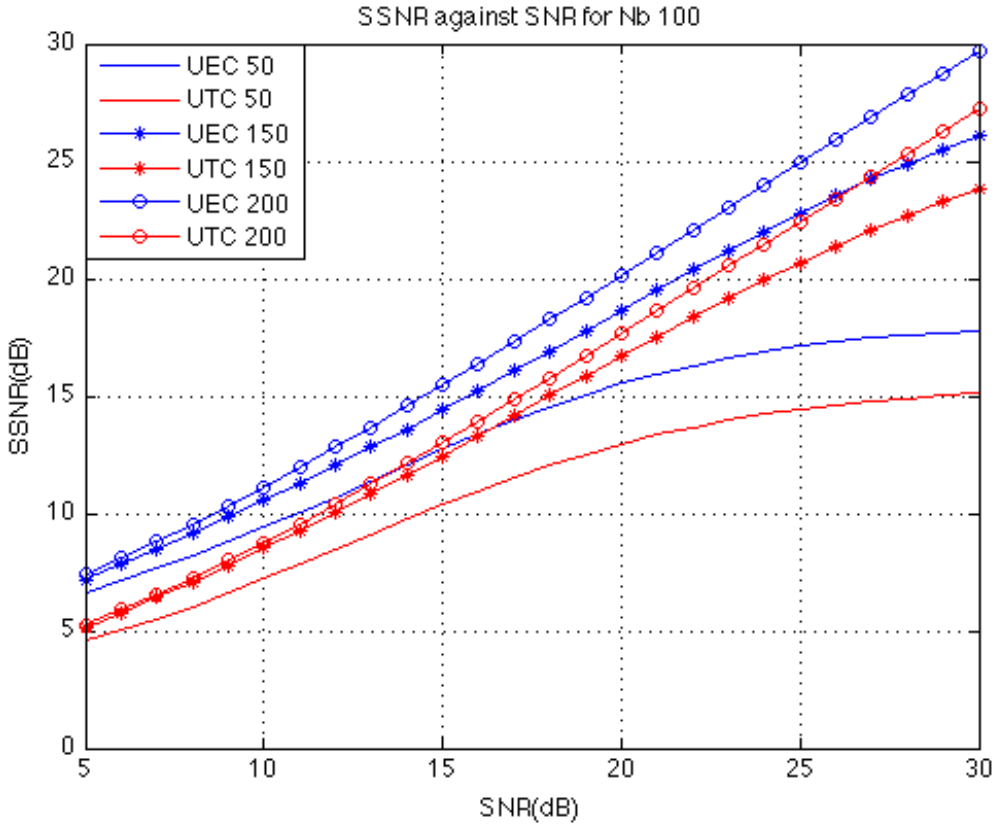

Figure 3.4: SSNR plots for different filter lengths.

increase as the filter length increase. This shows that the equalizers have to be sufficiently long to effectively shorten the channel. At the same filter length, UEC equalizers have higher SSNR than UTC equalizers. Figure 3.5 is the SSNR against relative delay plots for UEC. The relative delay that yields the highest SSNR is not always zero. Figures 3.6 is the SSNR against delay plot for UTC equalizer. For the same CIR, the optimal delay for both UEC and UTC can be different.

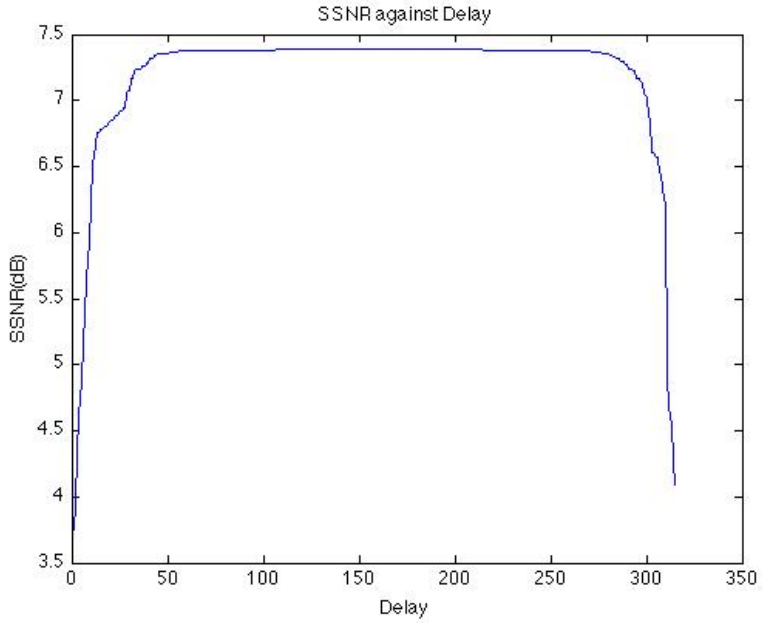

Figure 3.5: UEC SSNR against relative delay.

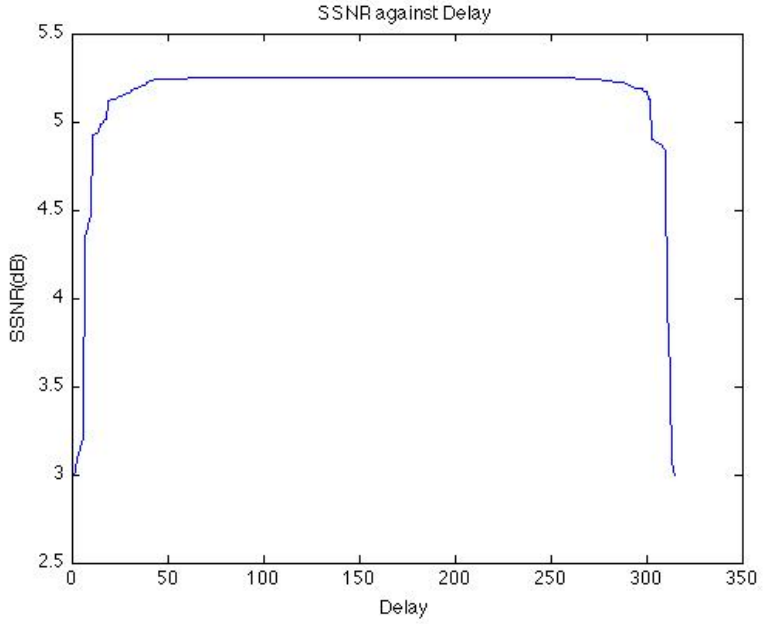

Figure 3.6: UTC SSNR against relative delay.

Figure 3.7 shows the Bit Error Rate (BER) to SNR plots of the different OFDM systems. As the CP length increases, the BER of OFDM with both

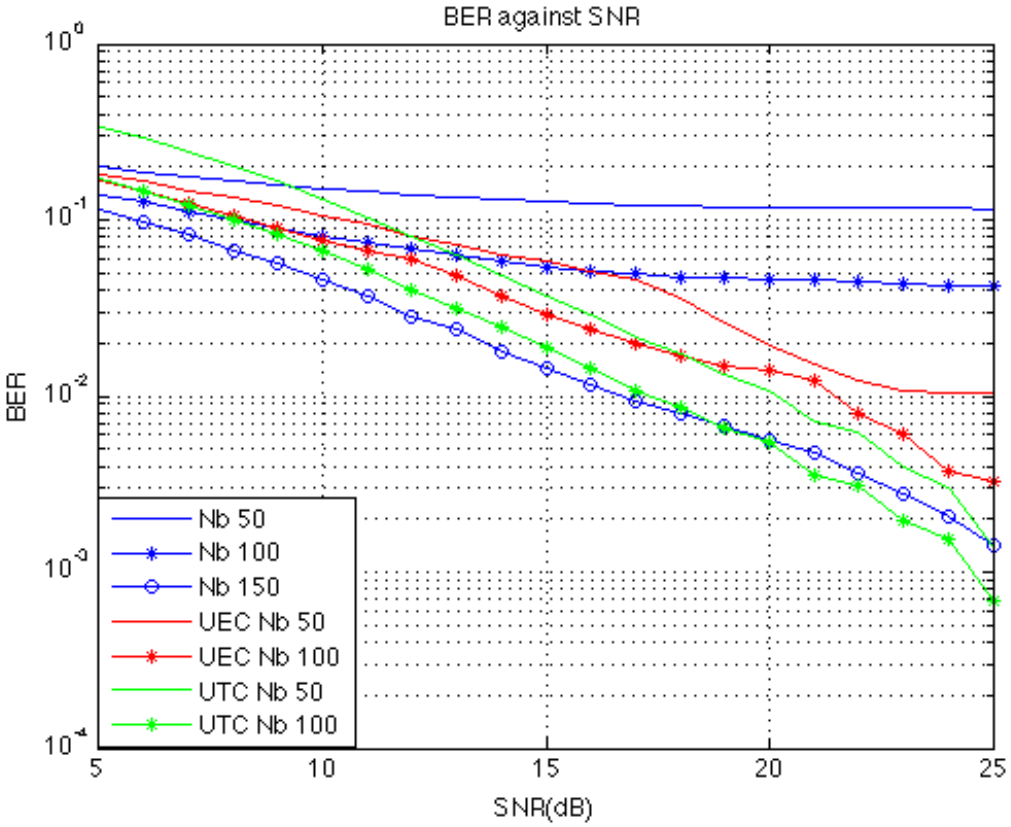

Figure 3.7: BER against SNR.

equalizers and OFDM without equalizer decreases. Even though the UEC CSE outperforms UTC CSE in terms of SSNR, UTC CSE has lower BER than UEC CSE. This is because the frequency response of the TIR for UEC has more deep nulls than UTC. At lower SNR, the sub-carriers which fall within these nulls have high error rate. Figure 3.8 shows the frequency responses and the bit error performances by sub-carrier of UEC and UTC in the three channels. Compared to UTC, the frequency response of UEC has more deep nulls. The error rate

performance of each sub-carrier is related to the frequency response.

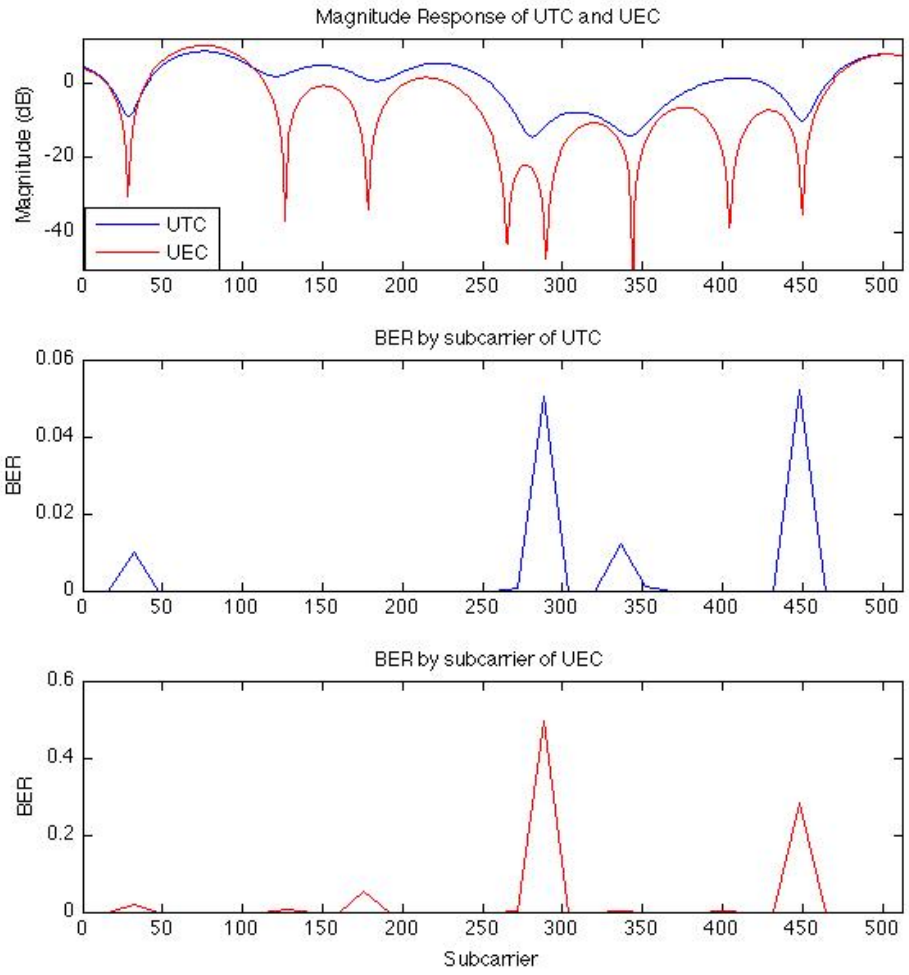

Figure 3.8: Frequency Responses and BER by sub-carriers.

Figure 3.9 is the plot of BER against Eb/No for different OFDM systems. The OFDM system with sufficiently long CP is used as a benchmark for the

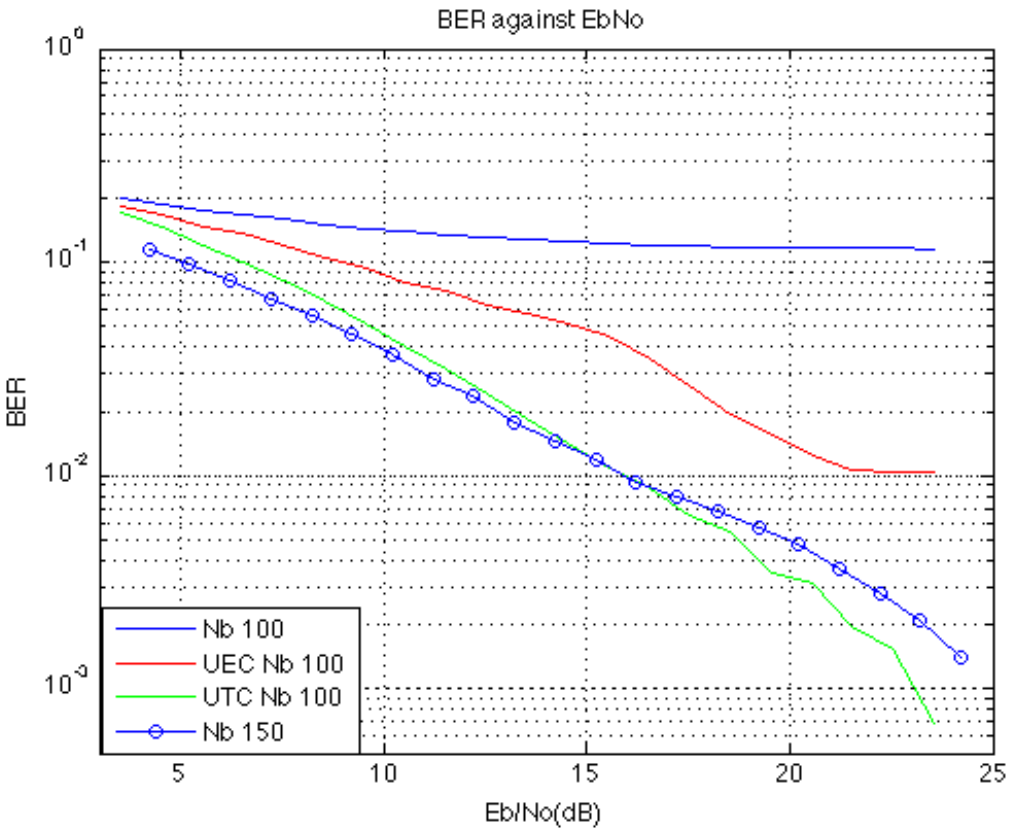

Figure 3.9: BER against Eb/No.

performance of the equalizers. For M-ary symbols, the E_b/N_o in dB is given by

$$E_b/N_o = SNR_{symbol} - 10\log_{10}(\log_2 M \times \frac{N_c}{N_c + N_p}) \tag{3.34}$$

where SNR_{symbol} is the SNR per channel symbol and N_p is the CP length. In the three plots, the BER performances of the OFDM with sufficient CP are included for comparison. The UTC equalizer with shorter CP performs almost as good as OFDM symbol with sufficiently long CP. The trend is consistent across the 3 channels.

Chapter 4

Time Domain Maximum Shortening Signal-to-Noise Ratio Channel Shortening Equalizers

4.1 MSSNR

Another method of performing channel shortening is the MSSNR [15]. From Figure 3.1 and equation 3.2 the output of the CSE can be expressed as

$$\begin{aligned} r[m] &= \mathbf{w}^H(\mathbf{H}\mathbf{x}[m] + \mathbf{n}[m]) \\ &= \mathbf{w}^H\mathbf{H}\mathbf{x}[m] + \mathbf{w}^H\mathbf{n}[m] \end{aligned} \tag{4.1}$$

From equation 4.1, assuming a noiseless scenario (zero forcing equalizer), we have

$$\begin{aligned} r_{zf}[m] &= \mathbf{w}^H \mathbf{H}\mathbf{x}[m] \\ &= \mathbf{x}[m]^H \mathbf{H}^T \mathbf{w} \\ &= \mathbf{x}[m]^H \mathbf{h}_{eff} \end{aligned} \tag{4.2}$$

Regardless of the choice of $\mathbf{w}$ there will be some energy that lies outside the largest N_b consecutive samples of $\mathbf{h}_{eff}$. Like the MMSE method, these samples do not have to start from the first sample. The energy that spills out of the N_b samples will contribute to ISI. The objective is to force as much of the energy to lie in N_b consecutive samples and hence minimizing the ISI and maximizing SSNR. We can break down h_{eff} from equation 4.2 into:

$$\begin{aligned} h_{eff} &= \mathbf{H}^T \mathbf{w} \\ &= \begin{bmatrix} h_{eff,0} \\ h_{eff,1} \\ \vdots \\ h_{eff,N_f+l-2} \end{bmatrix} \\ &= \begin{bmatrix} h_0 & 0 & \dots & & 0 \\ h_1 & h_0 & \ddots & & \\ \vdots & \vdots & & & \\ h_{N_f-1} & h_{N_f-2} & \dots & h_{N_f-l+1} & h_{N_f-l} \\ 0 & h_{N_f-1} & \dots & & h_{N_f-l+1} \\ \vdots & \ddots & & & \vdots \\ 0 & \dots & & 0 & h_{N_f-1} \end{bmatrix} \begin{bmatrix} w_0 \\ w_1 \\ \vdots \\ w_{N_f-1} \end{bmatrix} \end{aligned} \tag{4.3}$$

Let $\mathbf{h}_{win}$ represent a window of N_b consecutive samples of $\mathbf{h}_{eff}$ starting from a relative delay Δ and let $\mathbf{h}_{wall}$ be the remaining samples of $\mathbf{h}_{eff}$.

$$\begin{aligned}
\mathbf{h}_{win} &= \begin{bmatrix} h_{eff,\Delta} \\ h_{eff,\Delta+1} \\ \vdots \\ h_{eff,\Delta+N_b-1} \end{bmatrix} \\
&= \begin{bmatrix} h_{\Delta} & h_{\Delta-1} & \dots & h_{\Delta-N_f+1} \\ h_{\Delta+1} & h_{\Delta} & \dots & h_{\Delta-N_f+2} \\ \vdots & & \ddots & \vdots \\ h_{\Delta+N_b-1} & h_{\Delta+N_b-2} & \dots & h_{\Delta-N_f+N_b} \end{bmatrix} \begin{bmatrix} w_0 \\ w_1 \\ \vdots \\ w_{N_f-1} \end{bmatrix} \\
&\equiv \mathbf{H}_{win}\mathbf{w}
\end{aligned} \tag{4.4}$$

$$\begin{aligned}
\mathbf{h}_{wall} &= \begin{bmatrix} h_{eff,0} & \dots & h_{eff,\Delta-1} & h_{eff,\Delta+N_b} & \dots & h_{eff,N_f+l-2} \end{bmatrix}^T \\
&= \begin{bmatrix} h_0 & 0 & \dots & 0 \\ \vdots & \ddots & & \\ h_{\Delta-1} & h_{\Delta-2} & \dots & h_{\Delta-N_f} \\ h_{\Delta+N_b} & h_{\Delta+N_b-1} & \dots & h_{\Delta-N_f+N_b+1} \\ \vdots & \ddots & & \\ 0 & \dots & 0 & h_{l-1} \end{bmatrix} \begin{bmatrix} w_0 \\ w_1 \\ \vdots \\ w_{N_f-1} \end{bmatrix} \\
&\equiv \mathbf{H}_{wall}\mathbf{w}
\end{aligned} \tag{4.5}$$

The optimization problem is expressed as the choice of $\mathbf{w}$ to minimize $\mathbf{h}_{wall}^H\mathbf{h}_{wall}$ while imposing the constraint $\mathbf{h}_{win}^H\mathbf{h}_{win} = 1$. The constraint is imposed to avoid a

trivial zero solution. The expression of the energy outside and inside the window can be written as

$$\mathbf{h}_{wall}^{H}\mathbf{h}_{wall} = \mathbf{w}^{H}\mathbf{H}_{wall}^{H}\mathbf{H}_{wall}\mathbf{w} = \mathbf{w}^{H}\mathbf{A}\mathbf{w} \tag{4.6}$$

$$\mathbf{h}_{win}^{H}\mathbf{h}_{win} = \mathbf{w}^{H}\mathbf{H}_{win}^{H}\mathbf{H}_{win}\mathbf{w} = \mathbf{w}^{H}\mathbf{B}\mathbf{w} \tag{4.7}$$

The objective is to find $\mathbf{w}$ that minimizes $\mathbf{w}^{H}\mathbf{A}\mathbf{w}$ while keeping $\mathbf{w}^{H}\mathbf{B}\mathbf{w} = 1$. As long as $\mathbf{B}$ is positive definite, it can be decomposed using Cholesky decomposition [36] into

$$\begin{aligned} \mathbf{B} &= \mathbf{Q}\mathbf{\Lambda}\mathbf{Q}^{H} = \mathbf{Q}\sqrt{\mathbf{\Lambda}}\sqrt{\mathbf{\Lambda}}\mathbf{Q}^{H} \\ &= (\mathbf{Q}\sqrt{\mathbf{\Lambda}})(\mathbf{Q}\sqrt{\mathbf{\Lambda}})^{H} = \sqrt{\mathbf{B}}\sqrt{\mathbf{B}^{\mathbf{H}}} \end{aligned} \tag{4.8}$$

where $\mathbf{\Lambda}$ is a diagonal matrix formed of the eigenvalues of $\mathbf{B}$ and the columns of $\mathbf{Q}$ are the orthonormal eigenvectors. As long as $\mathbf{B}$ is of full rank, $(\sqrt{\mathbf{B}})^{-1}$ exists. In order to satisfy the constraint $\mathbf{w}^{H}\mathbf{B}\mathbf{w} = 1$,

$$\alpha = \sqrt{\mathbf{B}^{\mathbf{H}}}\mathbf{w} \tag{4.9}$$

such that

$$\alpha^{H}\alpha = \mathbf{w}^{H}\sqrt{\mathbf{B}}\sqrt{\mathbf{B}^{\mathbf{H}}}\mathbf{w} = \mathbf{w}^{H}\mathbf{B}\mathbf{w} = 1. \tag{4.10}$$

Solving for $\mathbf{w}$ in equation 4.10

$$\mathbf{w} = (\sqrt{\mathbf{B}^{\mathbf{H}}})^{-1}\alpha \tag{4.11}$$

we have

$$\mathbf{w}^H\mathbf{A}\mathbf{w} = \alpha^H(\sqrt{\mathbf{B}})^{-1}\mathbf{A}(\sqrt{\mathbf{B}^H})^{-1}\alpha = \alpha^H\mathbf{C}\alpha \tag{4.12}$$

From equations 4.8 and 4.12,

$$\mathbf{C} = (\mathbf{Q}\sqrt{\mathbf{\Lambda}})^{-1}\mathbf{A}(\sqrt{\mathbf{\Lambda}}\mathbf{Q}^H)^{-1} \tag{4.13}$$

Optimal shortening can thus be considered as choosing α to minimize $\alpha^H\mathbf{C}\alpha$ while constraining $\alpha^H\alpha = 1$. This solution occurs for $\alpha = \mathbf{l}_{min}$ where $\mathbf{l}_{min}$ is the unit-length eigenvector corresponding to the minimum eigenvalue λ_{min} of $\mathbf{C}$. The resulting equalizer coefficients are thus

$$\mathbf{w}_{opt} = (\sqrt{\mathbf{B}})^{-1}\mathbf{l}_{min} \tag{4.14}$$

In this model, Δ is searched exhaustively by finding the relative delay that yields the highest SSNR.This solution stays valid if $\mathbf{B}$ is invertible. In the scenario where the equalizer filter length is shorter than the CP length (i.e $N_b > N_f$) it holds. However, in a dispersive channel, in order to have an effective equalizer the filter length has to be sufficiently long. In [16], an alternative model is derived to allow a long equalizer (i.e $N_f > N_b$) to be implemented as a MSSNR CSE. Instead of minimizing $\mathbf{w}^H\mathbf{A}\mathbf{w}$ with $\mathbf{w}^H\mathbf{B}\mathbf{w} = 1$ constraint, the new approach tries to maximize $\mathbf{w}^H\mathbf{B}\mathbf{w}$ while keeping $\mathbf{w}^H\mathbf{A}\mathbf{w} = 1$. Equation 4.8 becomes

$$\begin{aligned} \mathbf{A} &= \mathbf{Q}\mathbf{\Lambda}\mathbf{Q}^H = \mathbf{Q}\sqrt{\mathbf{\Lambda}}\sqrt{\mathbf{\Lambda}}\mathbf{Q}^H \\ &= (\mathbf{Q}\sqrt{\mathbf{\Lambda}})(\mathbf{Q}\sqrt{\mathbf{\Lambda}})^H = \sqrt{\mathbf{A}}\sqrt{\mathbf{A^H}} \end{aligned} \tag{4.15}$$

Equation 4.8 to equation 4.13 have the $\mathbf{B}$ term replaced by $\mathbf{A}$ and vice versa. The equalizer coefficients are, hence:

$$\mathbf{w}_{opt} = (\sqrt{\mathbf{A}})^{-1}\mathbf{l}_{max} \tag{4.16}$$

where $\mathbf{l}_{max}$ is the unit-length eigenvector corresponding to the maximum eigenvalue λ_{max} of the new $\mathbf{C}$.

4.2 Generic MSSNR

The previous approach assumes that the transmitted sequence is white and the noise is absent. This is not always the case in UWA communication. A more generic model of MSSNR is needed. In [17], a model similar to MMSE is developed which embeds the input autocorrelation matrix $\mathbf{R}_{xx}$ and noise autocorrelation matrix $\mathbf{R}_{nn}$ into the equation. We define

$$[\mathbf{\Gamma}]_{m,n} = \delta(j-k-\Delta)\begin{cases} 0 \le j < N_f + l \\ 0 \le k < N_b - 1 \end{cases} \tag{4.17}$$

and equation 4.8 can be rewritten as

$$\begin{aligned} MSE &= \mathbf{b}^H\mathbf{\Gamma}^T\mathbf{R}_{xx}\mathbf{\Gamma}\mathbf{b} - \mathbf{b}^H\mathbf{\Gamma}^T\mathbf{R}_{xx}\mathbf{H}^H\mathbf{w} \\ &\quad -\mathbf{w}^H\mathbf{H}\mathbf{R}_{xx}\mathbf{\Gamma}\mathbf{b} + \mathbf{w}^H\mathbf{H}\mathbf{R}_{xx}\mathbf{H}^H\mathbf{w} + \mathbf{w}^H\mathbf{R}_{nn}\mathbf{w}. \end{aligned} \tag{4.18}$$

By minimizing MSE via partial differentiation with respect to $\mathbf{b}$ we get,

$$\begin{aligned} \mathbf{\Gamma}^T\mathbf{R}_{xx}\mathbf{\Gamma}\mathbf{b} &= \mathbf{\Gamma}^T\mathbf{R}_{xx}\mathbf{H}^H\mathbf{w} && (4.19) \\ \Rightarrow \mathbf{b}_{opt} &= \mathbf{\Gamma}^T\mathbf{H}^H\mathbf{w} && (4.20) \end{aligned}$$

Combining both equations 4.18 and 4.20,

$$\begin{aligned} MSE &= \mathbf{w}^H\mathbf{H}[\mathbf{\Phi}^T\mathbf{R}_{xx}\mathbf{\Phi} - \mathbf{\Phi}^T\mathbf{R}_{xx} - \mathbf{R}_{xx}\mathbf{\Phi} + \mathbf{R}_{xx}]\mathbf{H}^H\mathbf{w} \\ &\quad + \mathbf{w}^H\mathbf{R}_{uu}\mathbf{w} \\ &= \mathbf{w}^H\mathbf{H}\mathbf{\Psi}^T\mathbf{R}_{xx}\mathbf{\Psi}\mathbf{H}^H\mathbf{w} + \mathbf{w}^H\mathbf{R}_{uu}\mathbf{w} && (4.21) \end{aligned}$$

where $\mathbf{\Phi} = \mathbf{\Gamma}\mathbf{\Gamma}^T$, and $\mathbf{\Psi} = \mathbf{I} - \mathbf{\Phi}$. We minimize MSE subject to UEC.

$$\mathbf{b}^H\mathbf{b} = \mathbf{w}^H\mathbf{H}\mathbf{\Gamma}\mathbf{\Gamma}^T\mathbf{H}^H\mathbf{w} = 1. \quad (4.22)$$

The solution becomes

$$\Rightarrow \mathbf{w}_{opt} = \arg\min_{\mathbf{w}}\{\mathbf{w}^H\mathbf{H}\mathbf{\Psi}^T\mathbf{R}_{xx}\mathbf{\Psi}\mathbf{H}^H\mathbf{w} + \mathbf{w}^H\mathbf{R}_{uu}\mathbf{w}\} \quad (4.23)$$

such that $\mathbf{w}^H\mathbf{H}\mathbf{\Gamma}\mathbf{\Gamma}^T\mathbf{H}^H\mathbf{w} = 1$. This becomes a generalized eigen-problem like in MSSNR by [15]. Note that if the input sequence is white and in a high SNR region where the last term in equation 4.21 becomes zero, equation 4.23 becomes equation 4.6.

4.3 Minimum ISI

In [18], another form of MSSNR called the Min ISI is introduced. It factors in the SSNR of the sub-carriers when choosing the CSE coefficients. This frequency weighting places ISI into spectral regions of low SNR in effect maximizing the rate by applying the water-pouring algorithm. Let's look at the relationship between the auto-correlation sequence $r_{xx}(n)$ and the power spectral density $S_x(\omega)$.

$$r_{xx}(n) = \frac{1}{N_c} \sum_{i=0}^{N_c} S_x \left(\frac{2\pi i}{N_c} \right) e^{j(2\pi ni/N_c)}. \tag{4.24}$$

And

$$\begin{aligned} \mathbf{R}_{xx}(j,k) &= r_{xx}(j-k) \\ &= \frac{1}{N_c} \sum_{i=0}^{N_c} e^{j(2\pi ji/N_c)} S_x \left(\frac{2\pi i}{N_c} \right) e^{-j(2\pi ki/N_c)} \end{aligned} \tag{4.25}$$

Using the DFT vector,

$$\mathbf{q}_i = \begin{bmatrix} 1 & e^{j(2\pi ni/N_c)} & e^{j(2\pi n2i/N_c)} & \dots & e^{j(2\pi n(N_c-1)i/N_c)} \end{bmatrix}^H \tag{4.26}$$

We can write equation 4.25 as

$$\mathbf{R}_{xx} = \frac{1}{N_c} \sum_{i=0}^{N_c} \mathbf{q}_i S_x \left(\frac{2\pi i}{N_c} \right) \mathbf{q}_i^H. \tag{4.27}$$

Similarly,

$$\mathbf{R}_{uu} = \frac{1}{N_c} \sum_{i=0}^{N_c} \mathbf{q}_i S_n \left(\frac{2\pi i}{N_c} \right) \mathbf{q}_i^H. \tag{4.28}$$

Substituting equation 4.26 and equation 4.27 into equation 4.23 and ignoring the

scaling by $\frac{1}{N_c}$,

$$\begin{aligned}\mathbf{w}_{opt} = \ & \arg\min_{\mathbf{w}} \left(\mathbf{w}^H \mathbf{H} \mathbf{\Psi}^T \sum_{i=0}^{N_c} \mathbf{q}_i S_x \left(\frac{2\pi i}{N_c} \right) \mathbf{q}_i^H \mathbf{\Psi} \mathbf{H}^H \mathbf{w} \right. \\ & \left. + \mathbf{w}^H \mathbf{\Theta}^T \sum_{i=0}^{N_c} \mathbf{q}_i S_n \left(\frac{2\pi i}{N_c} \right) \mathbf{q}_i^H \mathbf{\Theta} \mathbf{w} \right) \end{aligned} \tag{4.29}$$

with the same UEC constraint.$\mathbf{\Theta}$ is the padding matrix for dimension matching. We define a new term P_d:

$$\begin{aligned} P_d \ &= \ \left(\mathbf{w}^H \mathbf{H} \mathbf{\Psi}^T \sum_{i=0}^{N_c} \mathbf{q}_i S_x \left(\frac{2\pi i}{N_c} \right) \mathbf{q}_i^H \mathbf{\Psi} \mathbf{H}^H \mathbf{w} \right. \\ & \quad \left. + \mathbf{w}^H \mathbf{\Theta}^T \sum_{i=0}^{N_c} \mathbf{q}_i S_n \left(\frac{2\pi i}{N_c} \right) \mathbf{q}_i^H \mathbf{\Theta} \mathbf{w} \right) \\ &= \ \left(\mathbf{w}^H \mathbf{H} \mathbf{\Psi}^T \sum_{i=0}^{N_c} \mathbf{q}_i S_{x,i} \mathbf{q}_i^H \mathbf{\Psi} \mathbf{H}^H \mathbf{w} \right. \\ & \quad \left. + \mathbf{w}^H \mathbf{\Theta}^T \mathbf{q}_i S_{n,i} \mathbf{q}_i^H \mathbf{\Theta} \mathbf{w} \right) \end{aligned} \tag{4.30}$$

After normalizing P_d with $S_{n,i}$, we derive a new objective function:

$$\begin{aligned} P_{d,norm} \ &= \ \mathbf{w}^H \mathbf{H} \mathbf{\Psi}^T \sum_{i=0}^{N_c} \mathbf{q}_i \left(\frac{S_{x,i}}{S_{n,i}} \right) \mathbf{q}_i^H \mathbf{\Psi} \mathbf{H}^H \mathbf{w} \\ & \quad + \mathbf{w}^H \mathbf{\Theta}^T \mathbf{q}_i \mathbf{q}_i^H \mathbf{\Theta} \mathbf{w} \end{aligned} \tag{4.31}$$

The last term becomes $\mathbf{w}^H \mathbf{w}$ and for a constant norm $\mathbf{w}$ it does not affect the minimization of equation 4.31. With UEC constraint, the solution becomes

$$\arg\min_{\mathbf{w}} \left(\mathbf{w}^H \mathbf{H} \mathbf{\Psi}^T \sum_{i=0}^{N_c} \mathbf{q}_i \left(\frac{S_{x,i}}{S_{n,i}} \right) \mathbf{q}_i^H \mathbf{\Psi} \mathbf{H}^H \mathbf{w} \right) \tag{4.32}$$

or simply

$$\arg\min_{\mathbf{w}} \mathbf{w}^H \mathbf{X} \mathbf{w} \tag{4.33}$$

where

$$\mathbf{X} = \mathbf{H}\mathbf{\Psi}^T \sum_{i=0}^{N_c} \left(\mathbf{q}_i \frac{S_{x,i}}{S_{n,i}} \mathbf{q}_i^H \right) \mathbf{\Psi}\mathbf{H}^H \tag{4.34}$$

If the transmitted signal is white, the frequency weighting of the algorithm depends on the noise. If the noise sequence is white, equation 4.32 will be identical to equation 4.6. Min ISI is a generalization of the MSSNR method. The constraints in both methods are identical. The MSSNR method minimizes the norm of the ISI path impulse response. Min ISI on the other hand minimizes a weighted sum of the ISI power. The weighting is with the individual sub-carrier SNR. Both methods would be identical if the subcarrier SNR were constant for all subcarriers and all subcarriers are used. According to [18], the frequency weighting amplifies the objective function in sub-carriers with high SNR. By reducing the ISI in high SNR sub-carriers, the SNR of these sub-carriers increase drastically. In sub-carriers with low SNR, the noise power is larger than ISI, hence the effect of ISI reduction on SNR and bit rate is small. The sub-carrier SNR can be defined as

$$SNR_i = \frac{\mathbf{w}^H \mathbf{H}\mathbf{\Gamma}\mathbf{q}_i S_{x,i} \mathbf{q}_i^H \mathbf{\Gamma}^T \mathbf{H}^H \mathbf{w}}{\mathbf{w}^H \mathbf{H}\mathbf{\Psi}^T \mathbf{q}_i S_{x,i} \mathbf{q}_i^H \mathbf{\Psi}\mathbf{H}^H \mathbf{w} + \mathbf{w}^H \mathbf{\Theta}^T \mathbf{q}_i S_{n,i} \mathbf{q}_i^H \mathbf{\Theta}\mathbf{w}} \tag{4.35}$$

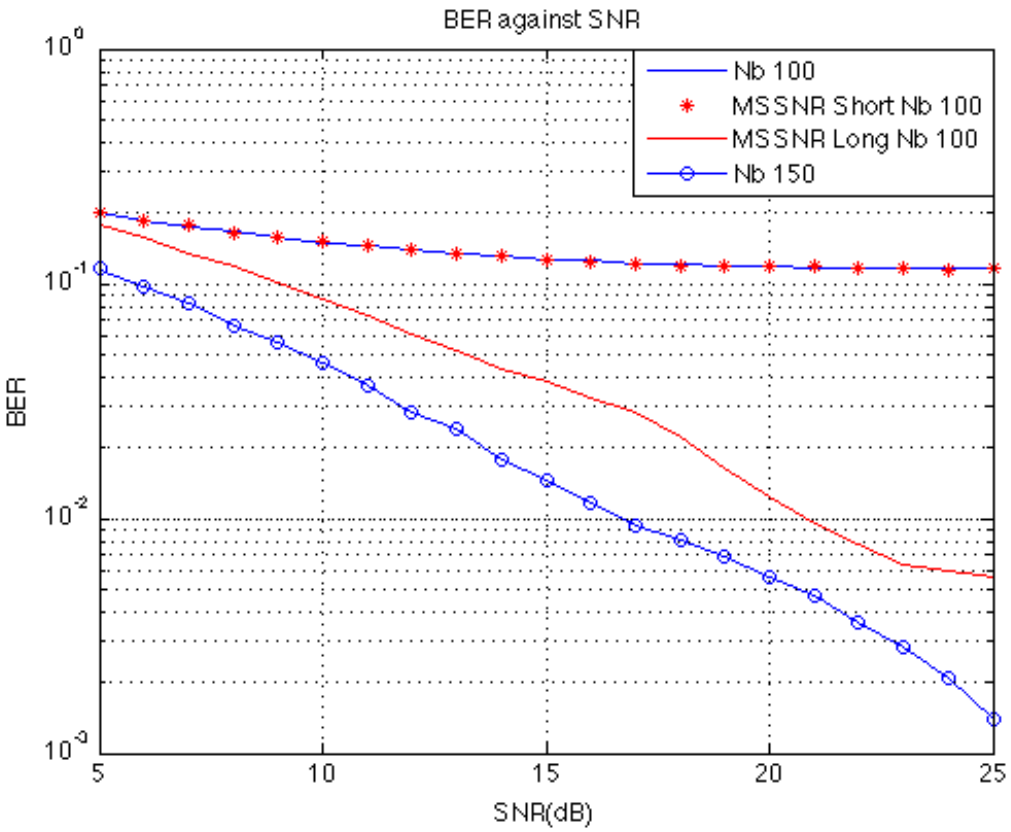

Figure 4.1: BER against SNR plot.

4.4 Simulation Results

The simulations on MSSNR use the same parameters as the simulations in the previous chapter. Figure 4.1 shows the plot of BER against SNR for two different MSSNR CSEs. The 'MSSNR Short' represents the MSSNR model in [15] and the 'MSSNR Long' represents MSSNR in [17]. For a channel with long delay spread, the filter length has to be long to effectively shorten the channel. If the filter length of the CSE is shorter than the CP length, the CSE will not be able to shorten the CIR, leaving large ISI outside the CP and causing high

number of error bits. The BER plot shows short filter length MSSNR is ineffective in shortening the channel. The same relative delay parameter is introduced in MSSNR just like in MMSE CSE as shown in Figure 4.2. The relative delay is a CIR dependent parameter. The delay corresponds to the highest SSNR is not necessarily zero. Figure 4.3 shows the BER against EbNo plots for MMSE and MSSNR. UTC performs the best in terms of BER. As the noise is white, Min ISI yield the same result as MSSNR. This is because the objective function of Min ISI reduces to MSSNR when the sub-carrier SNR is constant.

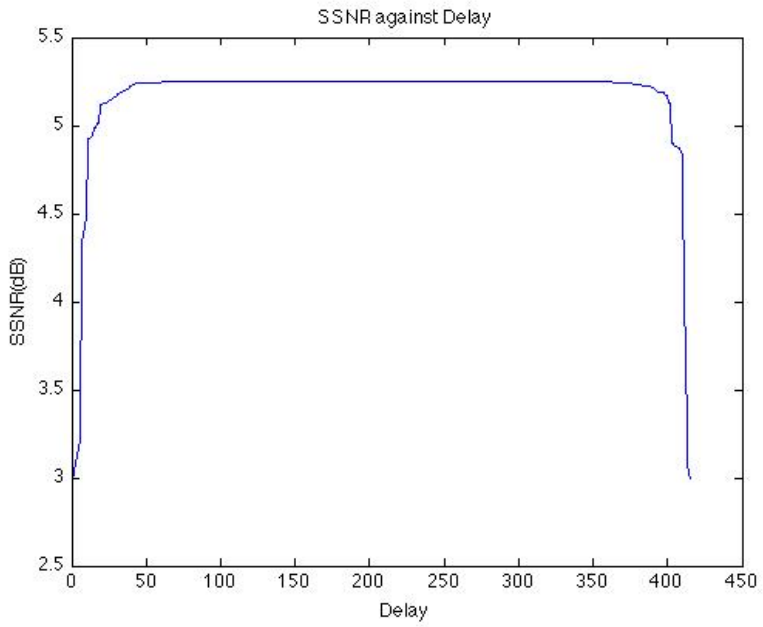

Figure 4.2: SSNR against Relative Delay.

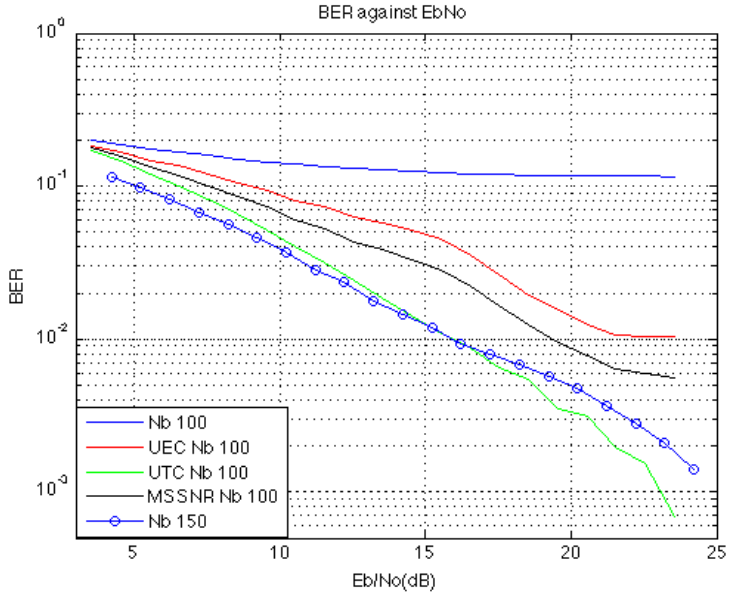

Figure 4.3: BER against EbNo plot

Figure 4.4 shows the power spectral density (PSD) of a colored noise. When the ratio of S_x/S_n is not constant across all sub-carriers, Min ISI will yield different result from MSSNR. From Figure 4.5, Min ISI outperforms MSSNR in terms of BER. This is because Min ISI is a frequency weighted solution of the CSE problem. For sub-carriers of high SNR, the BER performance depends on ISI. Hence by giving higher priority to sub-carriers with high SNR in eliminating ISI, the system achieves a better overall performance in BER.

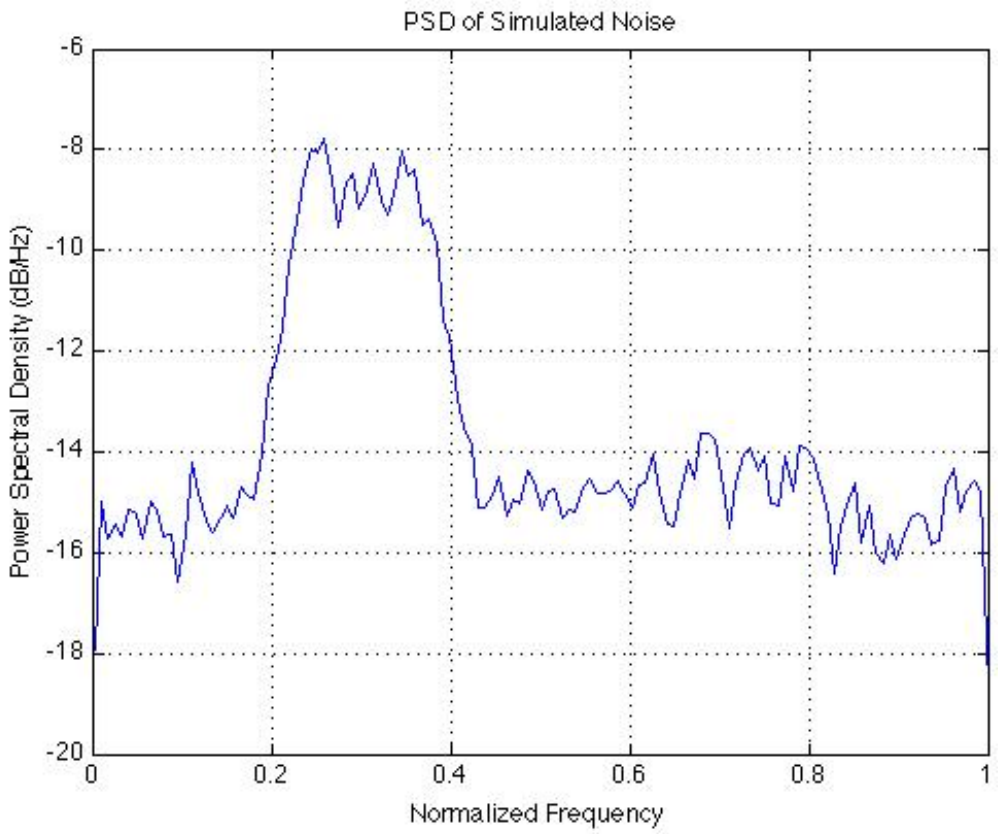

Figure 4.4: Colored Noise PSD

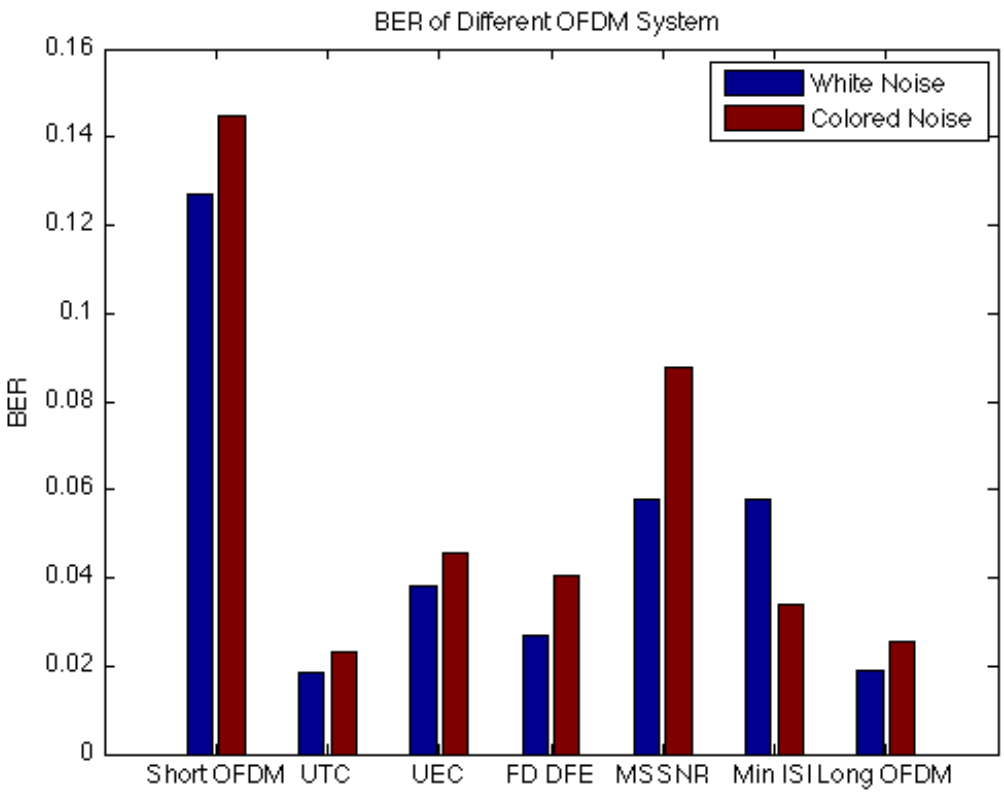

Figure 4.5: BER performance of equalizers in colored noise.

Chapter 5

Frequency Domain Decision Feedback Equalizer

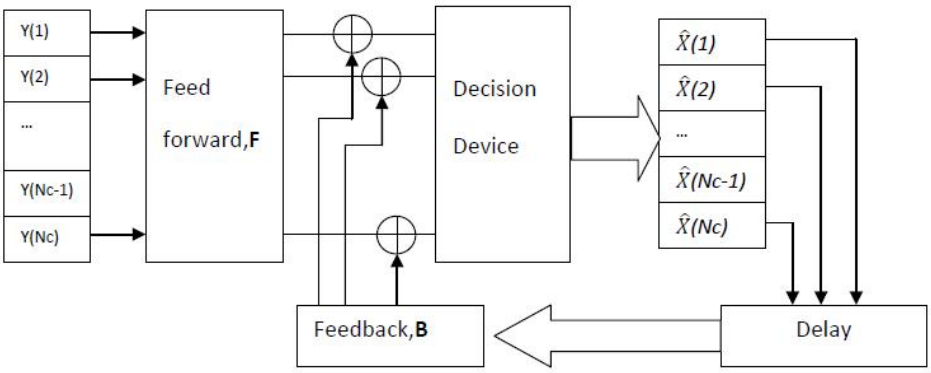

Figure 5.1: FD-DFE on OFDM

The Figure 5.1 shows how a FD-DFE works. Unlike the time domain CSEs, a FD equalizer for OFDM is applied to the symbols in frequency domain. Let $y(m)$ be the received symbol sequence. The current received symbol in the frequency

domain in subcarrier k is:

$$\begin{aligned} Y(k) &= FFT(y(m)) \\ &= \frac{1}{N_c}\sum_{m=0}^{N_c-1} y(m)e^{(-2\pi j)(m)(k)/N} \end{aligned} \tag{5.1}$$

and

$$Y(k) = Y_s(k) + Y_{ICI}(k) + Y_{ISI}(k) \tag{5.2}$$

where $Y_{ICI}(k)$ is the ICI portion of the received symbol, $Y_{ISI}(k)$ is the ISI portion of the received symbol and $Y_S(k)$ is the rest of the received symbol. In time domain, where i is the OFDM symbol index,

$$y_{ISI}(m) = \sum_{l=N_p+1}^{L-1} h(l)x_{i-1}(N_c - l + m + N_p)U(l - m - N_p - 1) \tag{5.3}$$

given

$$x_i(m) = \sum_{k=0}^{N_c-1} X(k)e^{(2\pi j)k/N_c}$$

Equation 5.3 becomes

$$\begin{aligned} y_{ISI}(m) &= \sum_{l=N_p+1}^{L-1} h(l)\sum_{q=0}^{N_c-1} X_{i-1}(q) \\ &\quad e^{(2\pi j)(N_c-l+m+N_p)/N_c}U(l - m - N_p - 1) \end{aligned} \tag{5.4}$$

$$\begin{aligned} Y_{ISI}(k) &= \frac{1}{N_c}\sum_{m=0}^{N_c-1}\sum_{l=N_p+1}^{L-1}\sum_{q=0}^{N_c-1} h(l)X_{i-1}(q) \\ &\quad e^{(2\pi j)(Nc-l+m+Np)/N_c}e^{(-2\pi j)(kq)/N_c}U(l - m - Np - 1) \end{aligned} \tag{5.5}$$

$U(n)$ is a unit step function where

$$U(n) = \begin{cases} 1 & n \geq 0 \\ 0 & n < 0 \end{cases}$$

$$\begin{aligned} y_{ICI}(m) &= \sum_{l=1}^{N_p} h(l+m)x_i(N_c - l + m)U(L-m-l) && (5.6) \\ &= \sum_{l=1}^{N_p} h(l+m) \sum_{q=0}^{N_c-1} X_i(q)e^{(2\pi j)(N_c-l+m)/N_c}U(L-m-l) && (5.7) \\ Y_{ICI}(k) &= \frac{1}{N_c} \sum_{m=0}^{L-1} \sum_{l=1}^{N_p} \sum_{q=0}^{N_c-1} h(l+m)X_i(q) \\ &\quad e^{(2\pi j)(Nc-l+m)/N_c}e^{(-2\pi j)(kq)/N_c}U(L-l-m) && (5.8) \end{aligned}$$

$$\begin{aligned} y_S(m) &= \sum_{l=0}^{L-1} h(l)x_i(m-l)U(m-l) && (5.9) \\ &= \sum_{l=0}^{L-1} h(l) \sum_{q=0}^{N_c-1} X_i(q)e^{(2\pi j)(m-l)/N_c}U(m-l) && (5.10) \\ Y_S(k) &= \frac{1}{N_c} \sum_{m=0}^{N_c-1} \sum_{l=0}^{L-1} \sum_{q=0}^{N_c-1} h(l)X_i(q) \\ &\quad e^{(2\pi j)(m-l)/N_c}e^{(-2\pi j)(kq)/N_c}U(l-m) && (5.11) \end{aligned}$$

Equation 5.2 can be expressed in a matrix notation as

$$\begin{aligned} \mathbf{Y} &= \mathbf{Y}_S + \mathbf{Y}_{ICI} + \mathbf{Y}_{ISI} + \mathbf{N} && (5.12) \\ &= \mathbf{C}_1\mathbf{X}_i + \mathbf{C}_2\mathbf{X}_i + \mathbf{S}\mathbf{X}_{i-1} + \mathbf{N}; && (5.13) \end{aligned}$$

where $\mathbf{Y}_S = \mathbf{C}_1\mathbf{X}_i$, $\mathbf{Y}_{ICI} = \mathbf{C}_2\mathbf{X}_i$, $\mathbf{Y}_{ISI} = \mathbf{S}\mathbf{X}_{i-1}$. $\mathbf{X}_i$ and $\mathbf{Y}_i$ are the transmitted symbol vector and received symbol vector in frequency domain, respectively. The elements in $\mathbf{S}$, $\mathbf{C}_1$ and $\mathbf{C}_2$, respectively, are:

$$\begin{aligned} S(k,q) &= \frac{1}{N_c}\sum_{m=0}^{N_c-1}\sum_{l=N_p+1}^{L-1} h(l)X_{i-1}(q)e^{(2\pi j)(Nc-l+m+Np)/N_c} \\ &\quad e^{(-2\pi j)(kq)/N_c}U(l-m-Np-1) \end{aligned} \tag{5.14}$$

$$\begin{aligned} C_1(k,q) &= \frac{1}{N_c}\sum_{m=0}^{N_c-1}\sum_{l=0}^{L-1} h(l)X_i(q)e^{(2\pi j)(m-l)/N_c} \\ &\quad e^{(-2\pi j)(kq)/N_c}U(l-m) \end{aligned} \tag{5.15}$$

$$\begin{aligned} C_2(k,q) &= \frac{1}{N_c}\sum_{m=0}^{L-1}\sum_{l=1}^{N_p} h(l+m)X_i(q)e^{(2\pi j)(Nc-l+m)/N_c} \\ &\quad e^{(-2\pi j)(kq)/N_c}U(L-l-m) \end{aligned} \tag{5.16}$$

The FD-DFE consists of a feedforward filter matrix and a feedback filter matrix, $\mathbf{W}$ and $\mathbf{B}$, respectively. The estimated symbol is:

$$\begin{aligned} \hat{X}_i(k) &= \mathbf{W}_k^H\mathbf{Y} - \mathbf{B}_k^H\hat{\mathbf{X}}_{i-1} \\ &= \begin{bmatrix} \mathbf{W}_k \\ -\mathbf{B}_k \end{bmatrix}^H \begin{bmatrix} \mathbf{Y} \\ -\hat{\mathbf{X}}_{i-1} \end{bmatrix} \end{aligned} \tag{5.17}$$

where $\hat{\mathbf{X}}_{i-1}$ is the predicted previous symbol. If the previous decisions are assumed to be correct. The MMSE Wiener-Hopf solution is implemented to mini-

mize $E[|\hat{X}_i(k) - X_i(k)|^2]$; The solution is

$$\begin{bmatrix} \mathbf{W}_k \\ -\mathbf{B}_k \end{bmatrix} = \mathbf{R}^{-1}\mathbf{P}_k \tag{5.18}$$

where

$$\mathbf{R} = E\left[\begin{bmatrix} \mathbf{Y} \\ -\mathbf{X}_{i-1} \end{bmatrix}\begin{bmatrix} \mathbf{Y} \\ -\mathbf{X}_{i-1} \end{bmatrix}^H\right] \tag{5.19}$$

$$\mathbf{P}_k = E\left[\begin{bmatrix} \mathbf{Y} \\ -\mathbf{X}_{i-1} \end{bmatrix} X_i^*(k)\right] \tag{5.20}$$

Given $\mathbf{C} = \mathbf{C}_1 + \mathbf{C}_2$, $[E[\mathbf{Y}\mathbf{Y}^H] = \mathbf{C}\mathbf{C}^H + \mathbf{S}\mathbf{S}^H + \delta^2\mathbf{I}$ and $E[\mathbf{Y}\mathbf{X}_i^H] = \mathbf{S}$

$$\mathbf{R} = \begin{bmatrix} \mathbf{C}\mathbf{C}^H + \mathbf{S}\mathbf{S}^H + \delta^2\mathbf{I} & -\mathbf{S} \\ -\mathbf{S}^H & \mathbf{I} \end{bmatrix}$$

$$\mathbf{P}_k = \begin{bmatrix} \mathbf{C}_k \end{bmatrix}$$

5.1 Simulation Results

Figure 5.2 shows the performance of FD-DFE on OFDM symbol with different CP lengths. As the CP length increases, the BER of both the OFDM symbol with and without FD DFE improves. Figure 5.3 is the overall comparison of various OFDM systems. UTC performs the best in terms of BER in the 3 channels. The BER performance of UTC in an insufficient CP OFDM is almost the same as the BER of a sufficient CP OFDM given the same E_b/N_o.

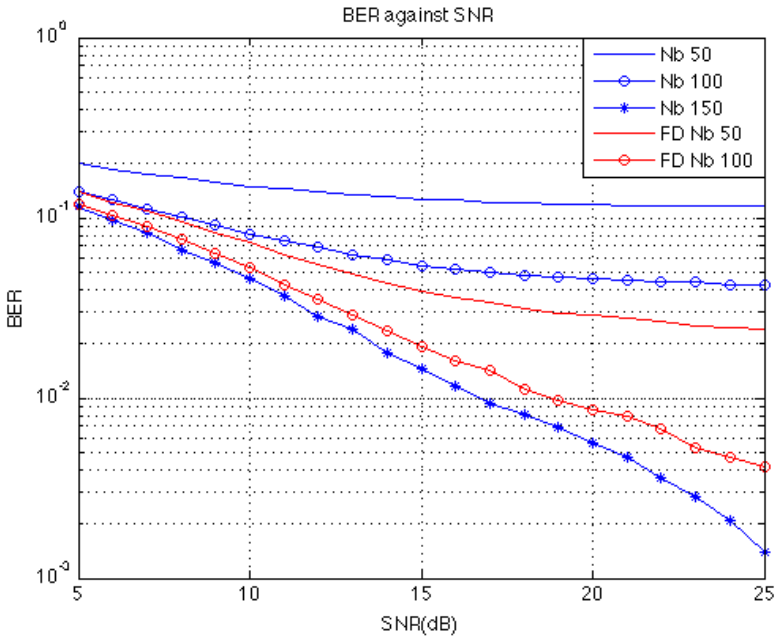

Figure 5.2: BER against SNR.

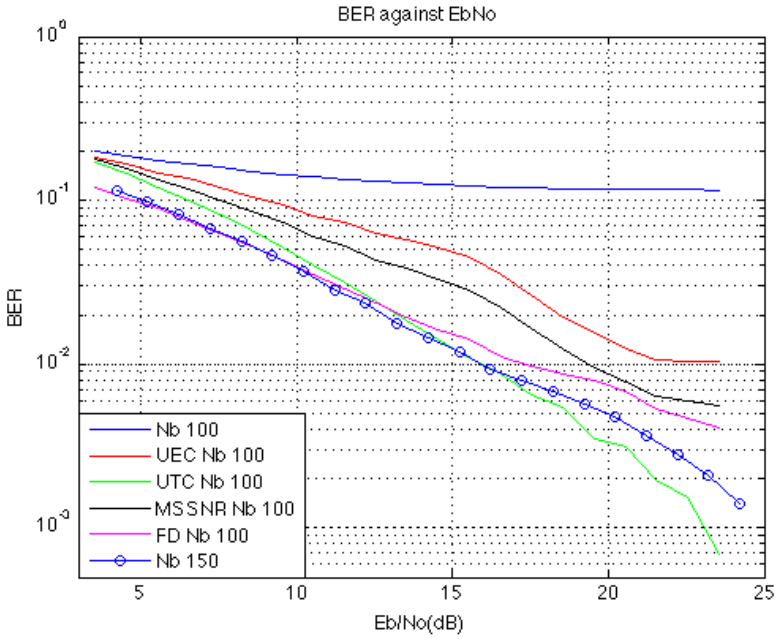

Figure 5.3: BER against EbNo

Chapter 6

Trial Data

For this thesis, the equalizers are based on non-adaptive channel estimate based methods. Recent results have shown the performance related advantages in computing the equalizer based on updated channel and noise estimates as opposed to updating the equalizer coefficients directly [12]. It is important to have a channel estimation that provides the most accurate channel parameters to the equalizers. In short and medium range shallow water acoustic communication, the channels more often than not have large delay spread and are time varying [37]. The CIRs tend to be sparse as well. Spareness is defined by the scenario where a big fraction of the channel energy is located in a small number of taps. A classic adaptive channel estimator like normalized least mean square (NLMS) and recursive least square (RLS) show poor performance in sparse and long channels for two reasons. First, the filter taps of NLMS and RLS will converge very slowly to their steady state values because the convergence rate of these algorithm are directly proportional to the channel length. Secondly, the steady state misadjustment would be high due to estimation noise from adaptation of low energy filter

taps. This calls for channel estimation algorithms that exploit the sparsity of the channel for better performance in steady state misadjustment value and convergence rate. There has been some work done on sparse estimation in the field of acoustic echo cancelation [38]. The improved proportionate NLMS (IPNLMS) and the improved proportionate affine projection algorithm (IPAPA) is shown to out-perform NLMS in channel estimation for echo cancelation. In recent years, some good results have been achieved on channel estimation for UWA channel by using these sparse adaptive natural gradient (NG) based algorithm [39; 40].

Channel estimation involves sending a known pilot sequence. This reduces the bandwidth efficiency because the pilot sequence does not carry any data. In our application, only the first symbol is known by the receiver for initialization of the channel estimation algorithm. Subsequently, we use the decoded bits as the pilot for channel estimation. The decoded symbols in the frequency domain is IFFT modulated into an OFDM time domain signal. The CIR estimated is used to calculate the equalizer coefficients for the subsequent received OFDM symbol. Figure 6.1 shows the flowchart of the decoding and channel estimation process.

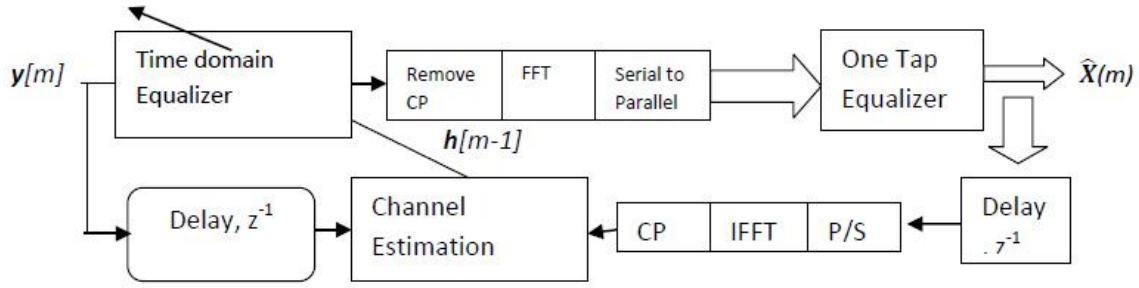

Figure 6.1: Processing of the received data

6.1 GLINT 08

During the GLINT 08 trials in August 2008, OFDM signals were transmitted (source level 175 dB re 1 μPa @ 1m) from a transducer mounted on a rigid pole deployed through a moon pool on the Leonardo (about 3.75 m below the hull). The signals were received on three hydrophones on a moored vertical array and recorded. The signals were repeated every 30 seconds for several hours as Leonardo moved as shown in Figure 6.2. The results from the hydrophones are averaged to have more accurate results by having different noise realizations.

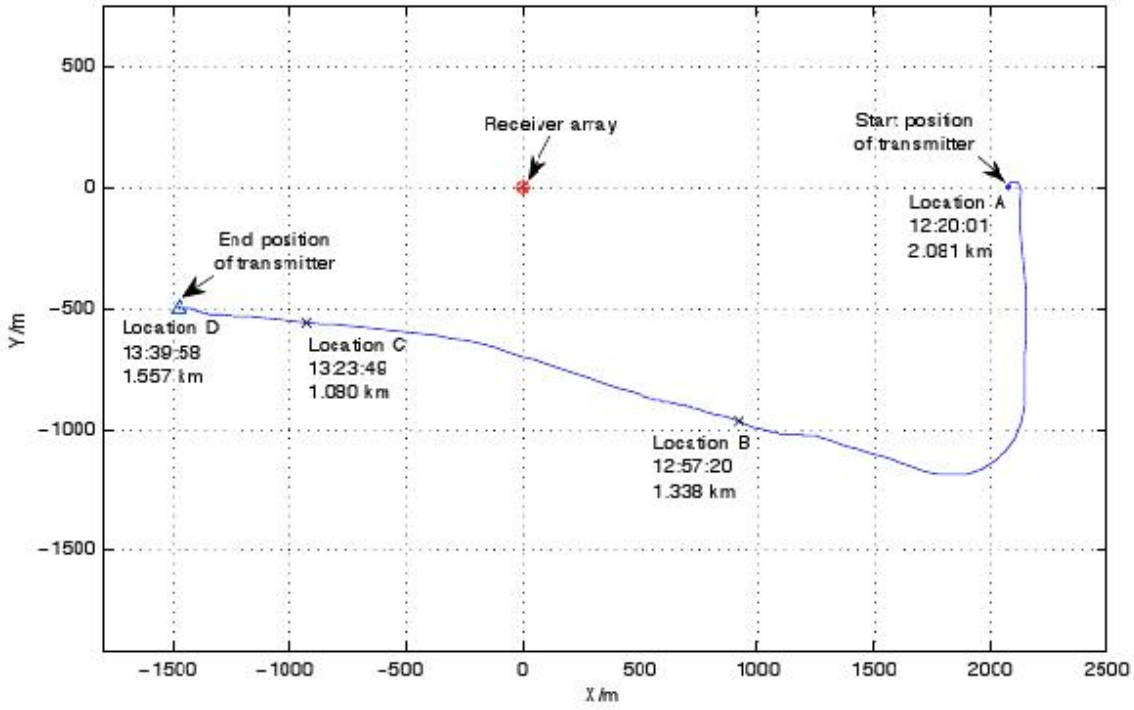

Figure 6.2: Motion of the transmitter with respect to a fixed receiver array (arbitrary coordinate system)

The spectrogram of the signals received at location D is shown in Figure 6.3.

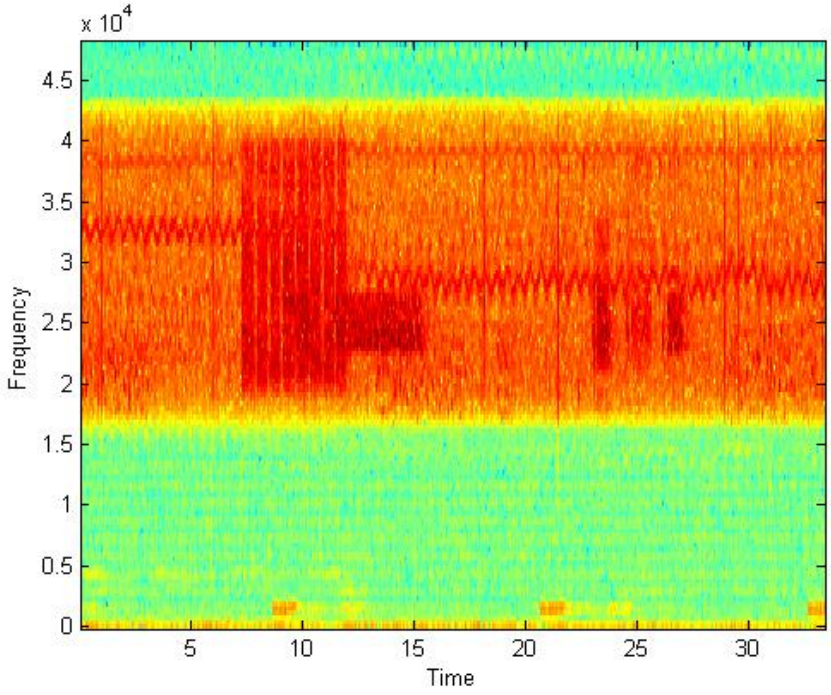

Figure 6.3: Spectrogram of received signal at D

The signals have been bandpass filtered from 18 kHz to 42 kHz to remove out-of-band interference and down-sampled to 96 kSa/s to reduce computational load. The OFDM signals transmitted have different number of sub-carriers N_c and CP length N_p. For better appreciation of the impact of ISI and the importance of the CSEs, two OFDM signals with short N_p are chosen for analysis in this section. The SNR is about 15-20 dB at low frequencies and decreases with frequency due to increased absorption. An average estimate of 14 dB SNR is computed from the signal and noise samples.

6.1.1 Signal 1

Figure 6.4 shows the snapshots of the estimated CIR for signal 1. The parame-

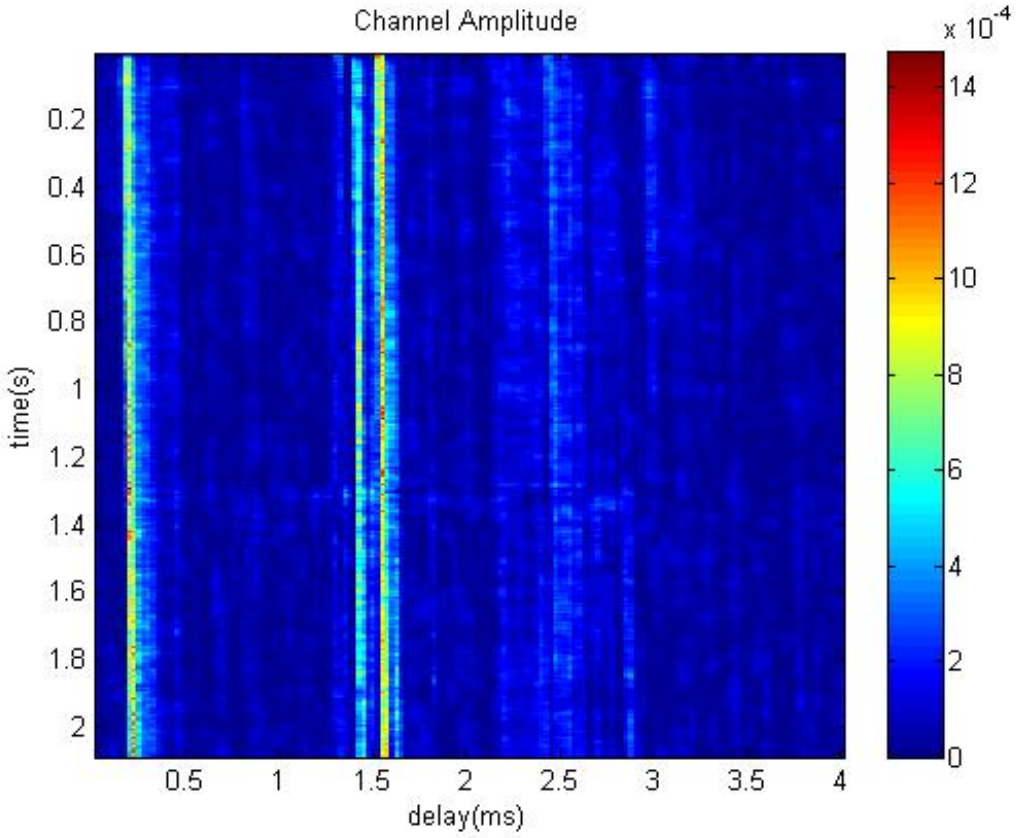

Figure 6.4: Snapshots of the estimated time-varying channel impulse response for GLINT 08 Signal 1. The horizontal axis represents delay, the vertical axis represents absolute time and the colorbar represents the amplitude. The intensity ranges linearly.

ters of signal 1 are shown in table 6.1. With a CP length of 0.8 ms, the OFDM signal will suffer from ISI because the a significant portion of the channel energy lies outside of the CP. From the estimated CIR we can deduce that this is a relatively sparse channel. Hence for faster convergence and more accurate steady state estimation, we can use IPNLMS or IPAPA. From Figure 6.5, IPAPA and IPNLMS outperform the other non-sparse algorithm in terms of convergence speed and steady state estimation error. The estimated CIR and the effective

Table 6.1: OFDM Parameters of Signal 1

N_c	256
N_p	16
N_s	2
F_s	96000 Hz
F_d	20000 Hz
F_c	30000 Hz
Symbol Length	30

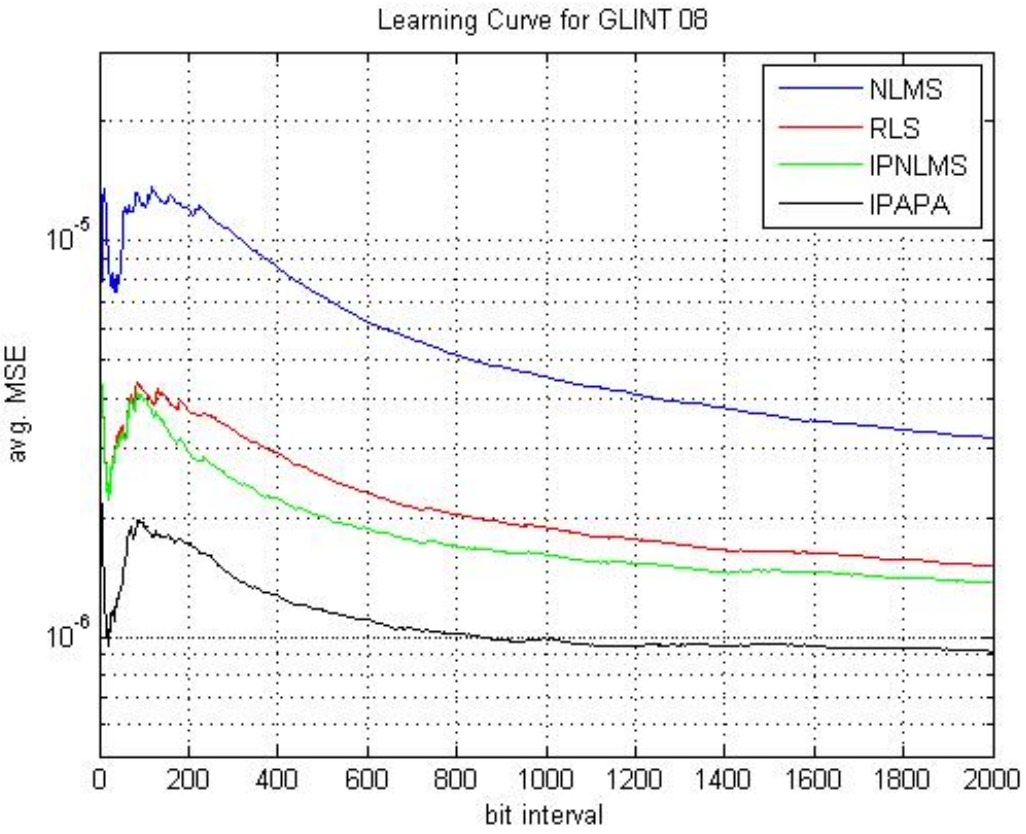

Figure 6.5: Learning Curve for Signal 1

CIR of the signal is shown in Figure 6.6. The length of the effective CIR with CSE is shorter than the CP. Figure 6.7 shows the carrier phase estimate which is done in conjunction with channel estimation using second order phase-locked loop (PLL) [41]. The estimated phase is then fed to the equalizer to correct for residual carrier phase.

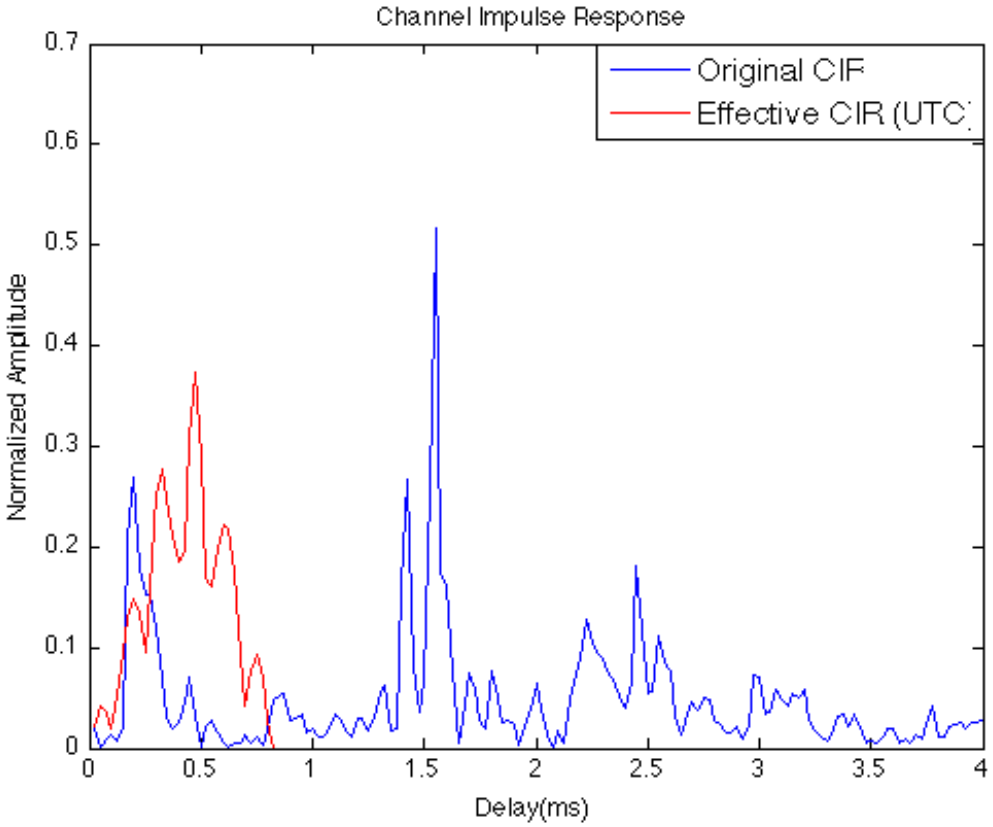

Figure 6.6: Effective CIR and original CIR of GLINT 08 signal 1.

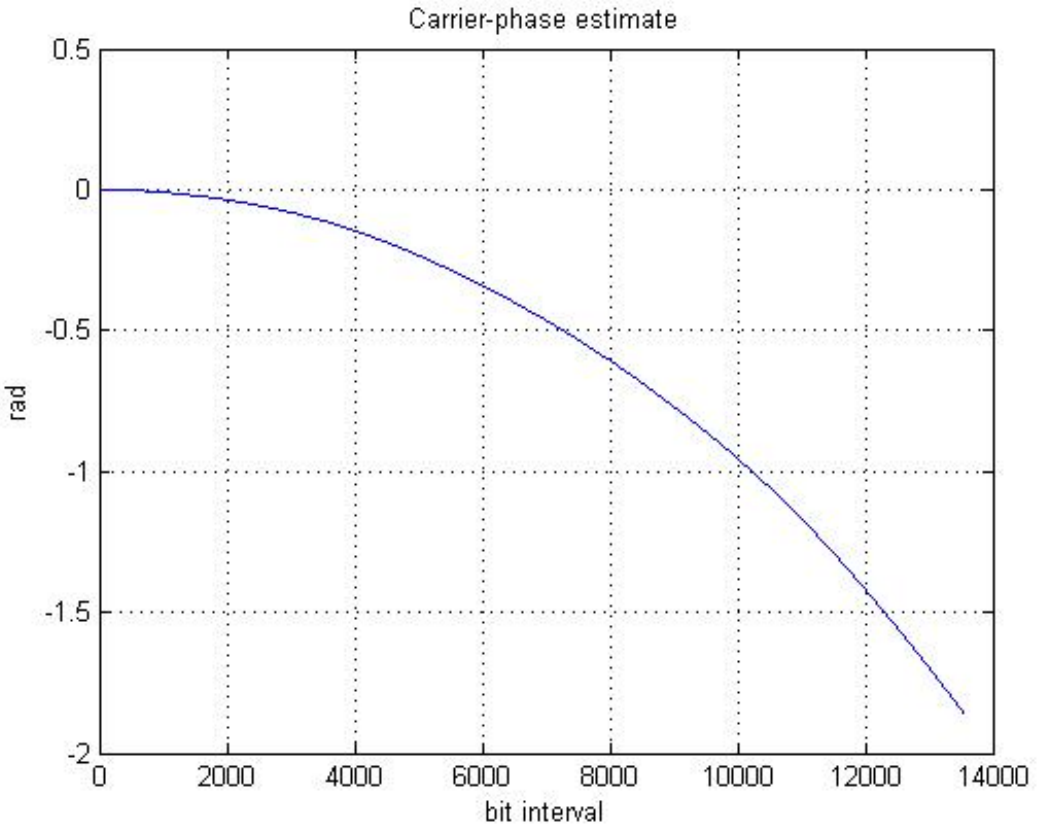

Figure 6.7: Carrier Phase Estimate for Signal 1

Table 6.2 shows the BER performance of different equalizers. 'OFDM' represents the OFDM signal without equalizer. Since the CIR is time-varying, the channel has to be continuously tracked in order to have the correct equalizer filter coefficients. In our case, we use the previously decoded OFDM symbol as the pilot signal to the channel estimator. To reduce the BER, a rate 1/3 convolution encoding is performed at the transmitter. The first column of Table 6.2 assumes perfect decoding, i.e., the actual transmitted signal was used as a pilot. The second column is based on pilot generated from the decoder output (decision directed). In both cases, the BER performance of OFDM is worse than

Table 6.2: BER performance in Signal 1

Method	Perfect Feedback	Imperfect Feedback	Imperfect Feedback (Code 1/3 rate)
OFDM	0.1473	0.1548	0.0323
UTC	0.0932	0.1104	0.0021
UEC	0.1273	0.1431	0.0227
MSSNR	0.1224	0.1337	0.0097
MIN ISI	0.1235	0.1357	0.0094
FD DFE	0.1123	0.1245	0.0054
Bit Rate (kbits/s)	37.4	37.4	12.4

the rest. UTC performs better than UEC because of the presence of deep nulls in the TIR of the UEC method. The BER performance of Min ISI is the same as MSSNR because the noise is white. In the imperfect feedback scenario, the decoding errors render the pilot signal inaccurate and thus leads to poorer channel estimation in the next OFDM period and degradation in the BER performance. Imperfect feedback rate 1/3 has lower BER than perfect feedback at the expense of reduced bit-rate. UTC performs better than UEC because of the deep nulls in the frequency response in TIR of UEC. Figure 6.9 illustrates this point clearly.

6.1.2 Signal 2

Table 6.3 shows the OFDM parameters of Signal 2. The CIR in Signal 2 is similar to Signal 1 because the gap between the two signals is small. Figures 6.10, 6.11, 6.12 and 6.13 show snapshots of the estimated CIR, learning curve, estimated CIR and estimated carrier phase respectively. The CIR of Signal 2 is sparse. IPNLMS and IPAPA are used to get a better channel estimation.

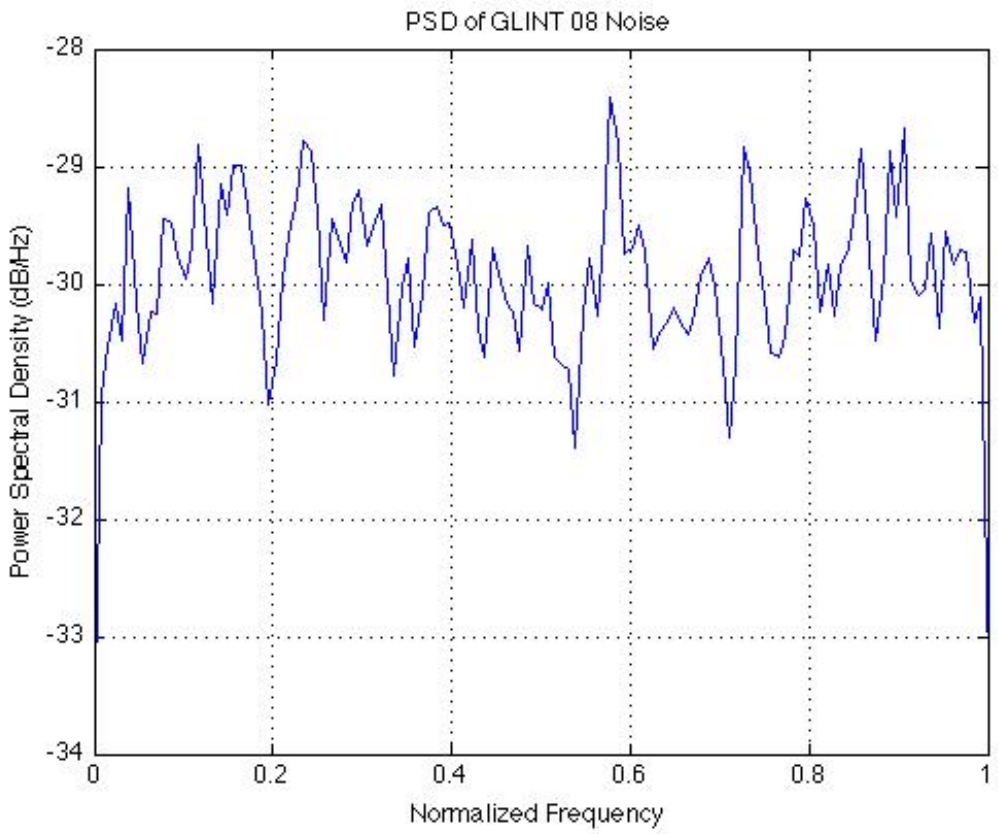

Figure 6.8: PSD of Noise for GLINT 08

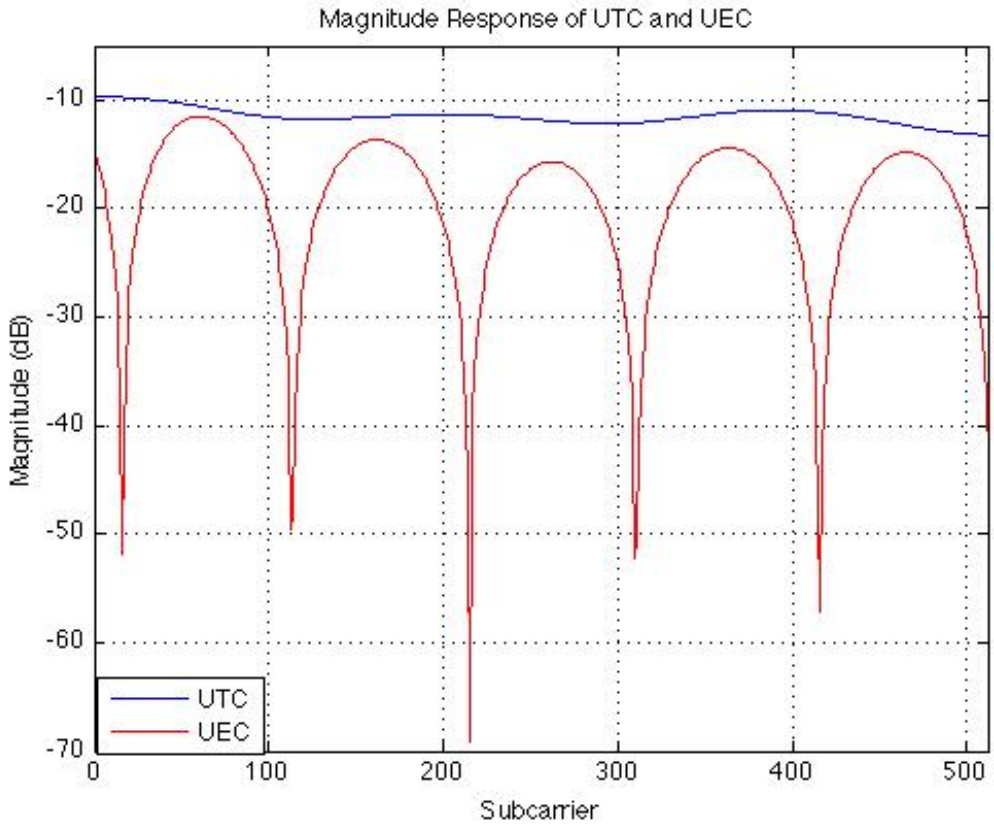

Figure 6.9: Frequency Response of TIR UEC and UTC for Signal 1

Table 6.3: OFDM Parameters of Signal 2

N_c	512
N_p	16
N_s	2
F_s	96000 Hz
F_d	20000 Hz
F_c	30000 Hz
Symbol Length	30

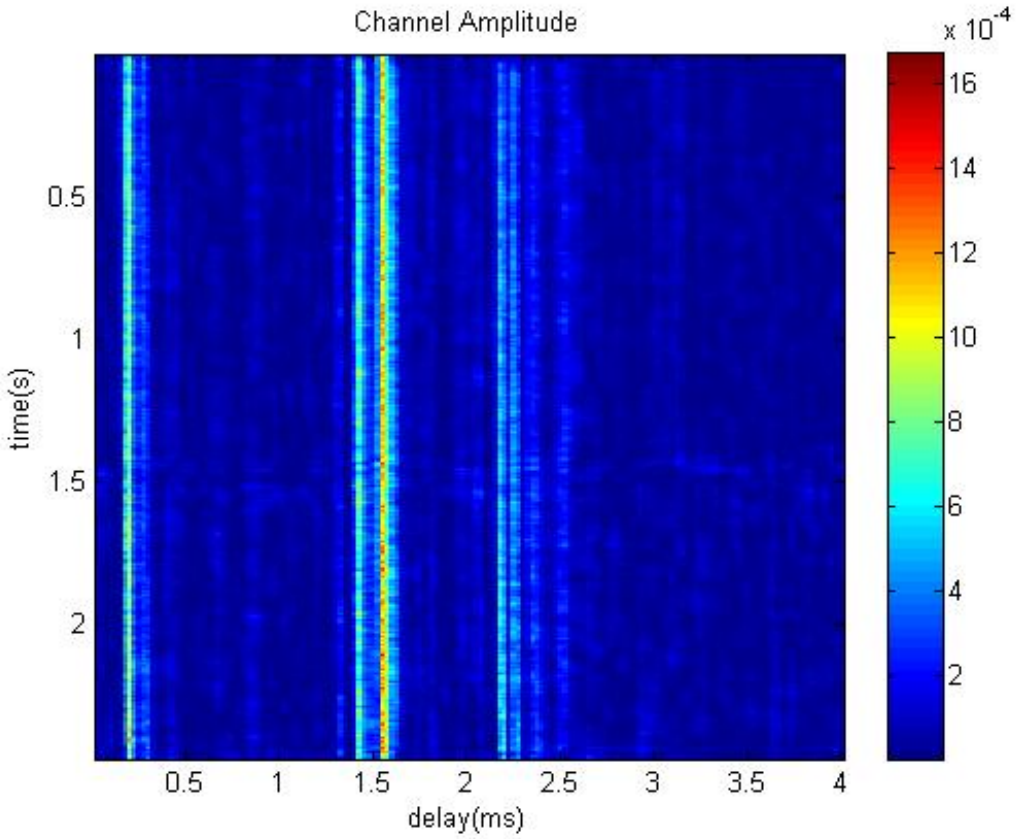

Figure 6.10: Snapshots of the estimated time-varying channel impulse response for GLINT 08 Signal 2. The horizontal axis represents delay, the vertical axis represents absolute time and the colorbar represents the amplitude. The intensity ranges linearly.

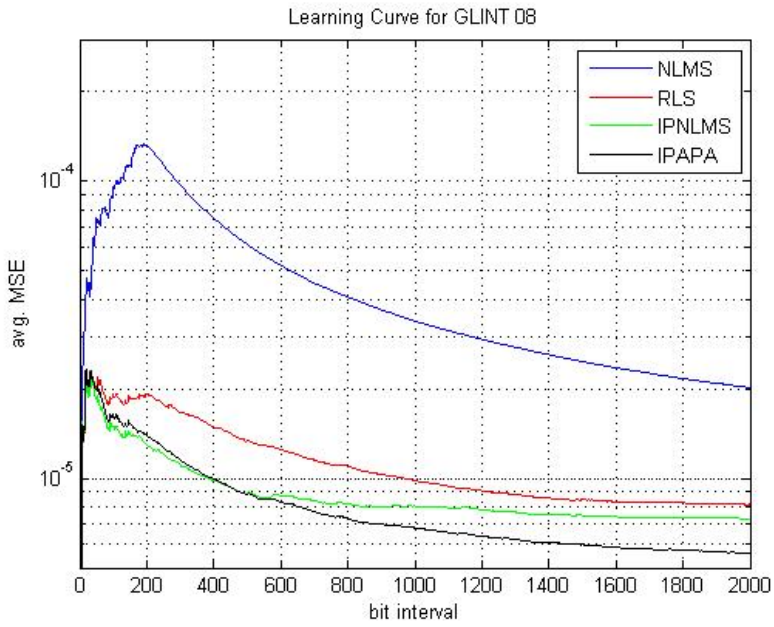

Figure 6.11: Learning Curve for Signal 2

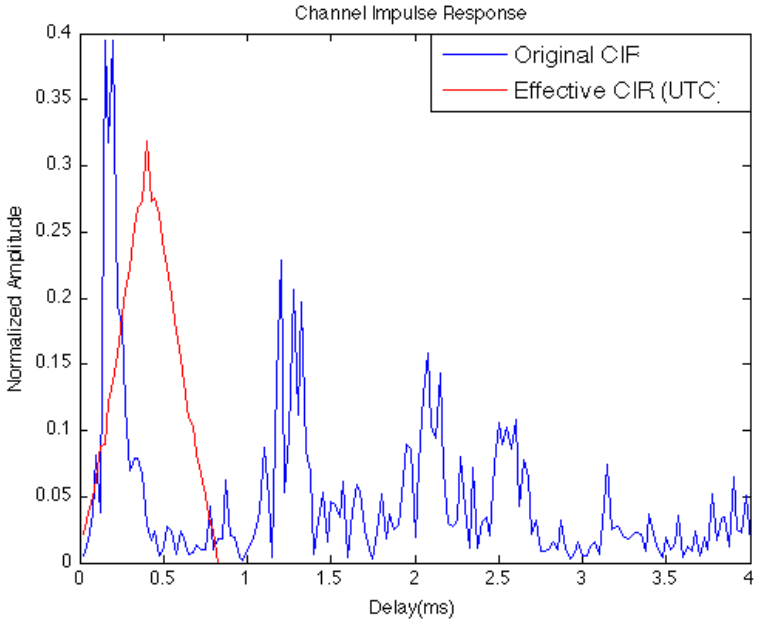

Figure 6.12: Effective CIR and original CIR of GLINT 08 signal 2.

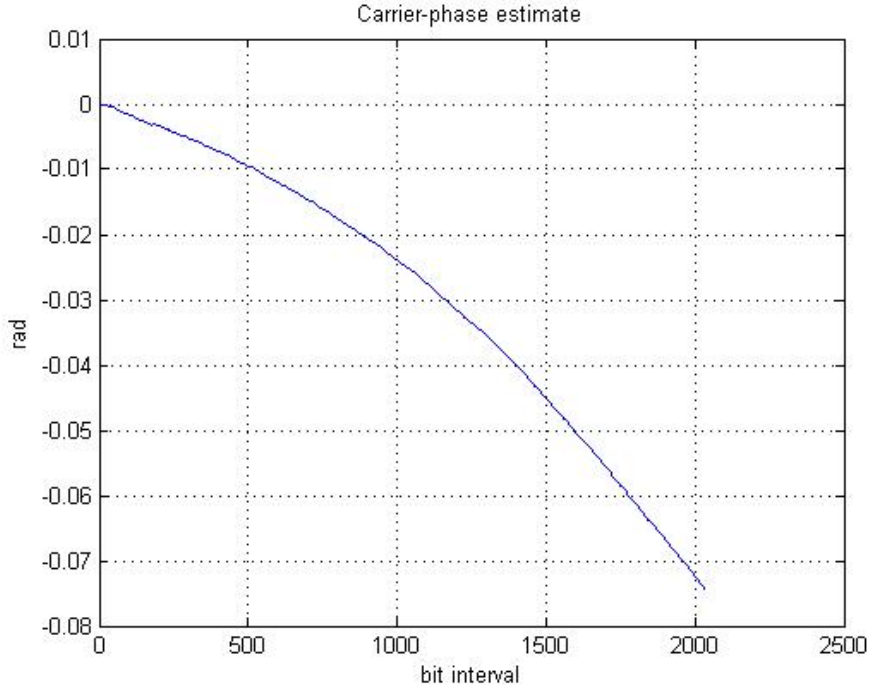

Figure 6.13: Carrier Phase Estimate for Signal 2

Table 6.4 shows the BER result of different equalizers. Similar to previous

Table 6.4: BER performance of Signal 2

Method	Perfect Feedback	Imperfect Feedback	Imperfect Feedback (Code 1/3 rate)
OFDM	0.1227	0.1354	0.0174
UTC	0.0724	0.1031	0.0017
UEC	0.1178	0.1542	0.0153
MSSNR	0.0889	0.1382	0.0093
MIN ISI	0.0901	0.1377	0.0085
FD DFE	0.0901	0.1421	0.0074
Bit Rate (kbits/s)	38.7	38.7	12.8

signal, UTC performs better than the rest of the equalizers. By encoding the

transmit symbols, the channel estimation and BER performance improve in the expense of the bit rate. The bit rate of Signal 2 is higher than Signal 1 due to higher number of sub-carriers transmitted. As the noise is white, Min ISI does not have an frequency advantage over MSSNR. Figures 6.14 shows the frequency responses of TIR of UEC and UTC respectively. At low SNR, the sub-carriers of the deep frequency response null have high BER due to detection error in noisy environment. There are more deep nulls in the frequency response of the TIR of UEC than UTC.

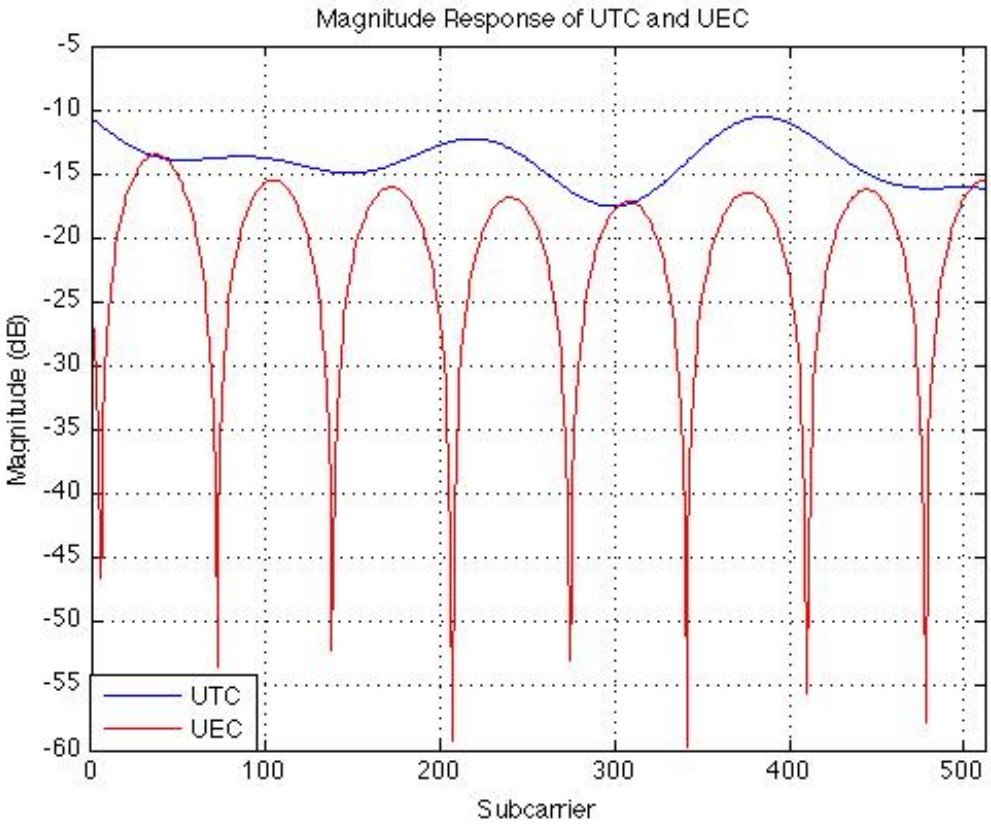

Figure 6.14: Frequency Response of TIR UEC and UTC for Signal 2

6.2 Singapore Water 2010

Table 6.5 shows the OFDM parameters of the signal.

Table 6.5: OFDM Parameters of Singapore Water 2010

N_c	256
N_p	10
F_s	200000 Hz
F_d	5000 Hz
F_c	27500 Hz
Symbol Length	30

The experimental data have been recorded in the area of Selat Pauh in Singapore waters on April 21st, 2010. Both the transmitter and the receiver were mounted on rigid tripods, 4m above the sea floor. The sea depth is 15m and the horizontal range of the link is 350m. The sound speed profile is isovelocity 1540m/s and the sea surface was calm during the experiment. The received average SNR is 11.5 dB. Of the 256 subcarriers, 129 subcarriers carried data. The rest are reserved for Peak-to-Average Power Ratio (PAPR) or are null carriers. Figures 6.15, 6.16 and 6.17 show snapshots of estimated CIR, a single capture of the estimated CIR and estimated carrier phase respectively. The CP at 2ms is clearly inadequate for the long CIR.

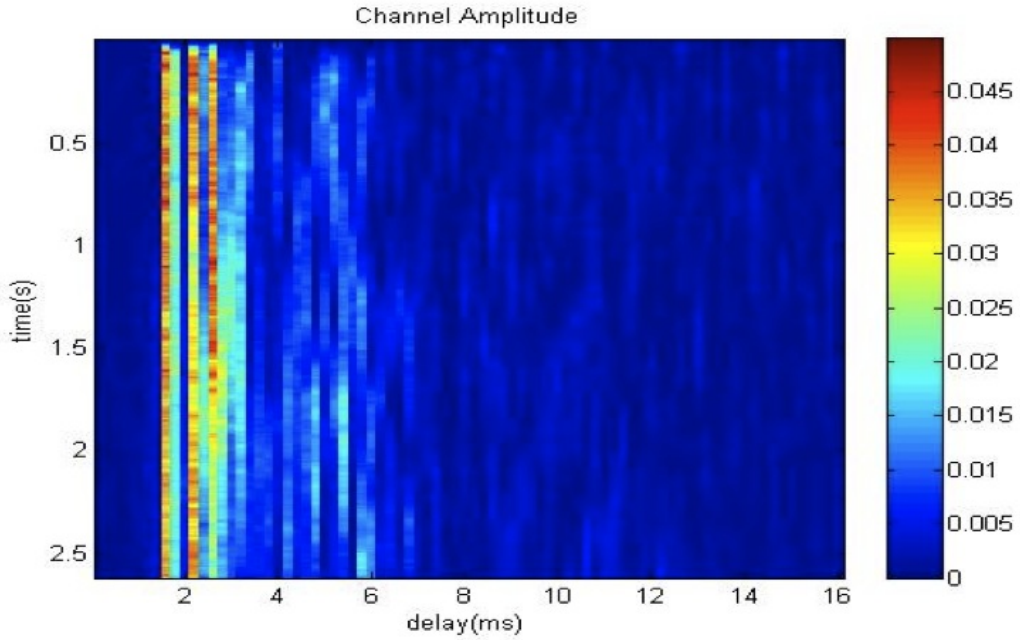

Figure 6.15: Snapshots of the estimated time-varying channel impulse response for Singapore Water 2010. The horizontal axis represents delay, the vertical axis represents absolute time and the colorbar represents the amplitude. The intensity ranges linearly.

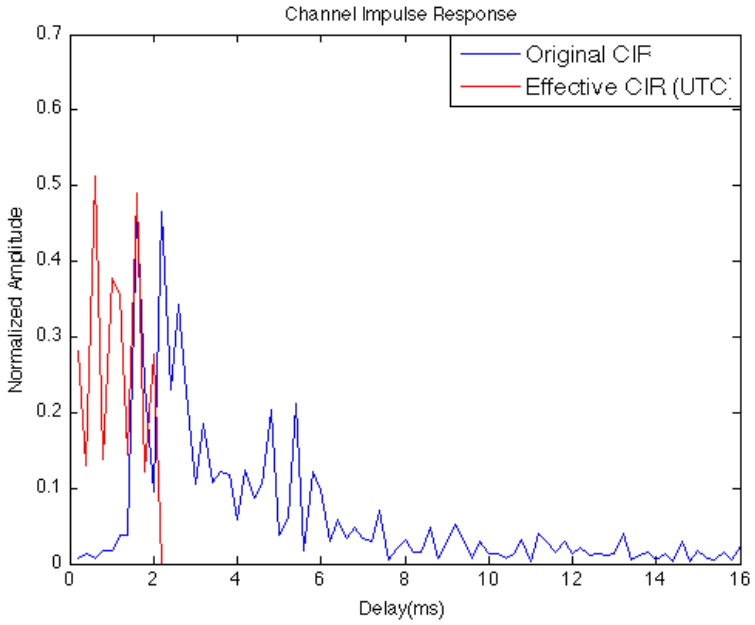

Figure 6.16: Effective CIR and original CIR of Singapore Water 2010.

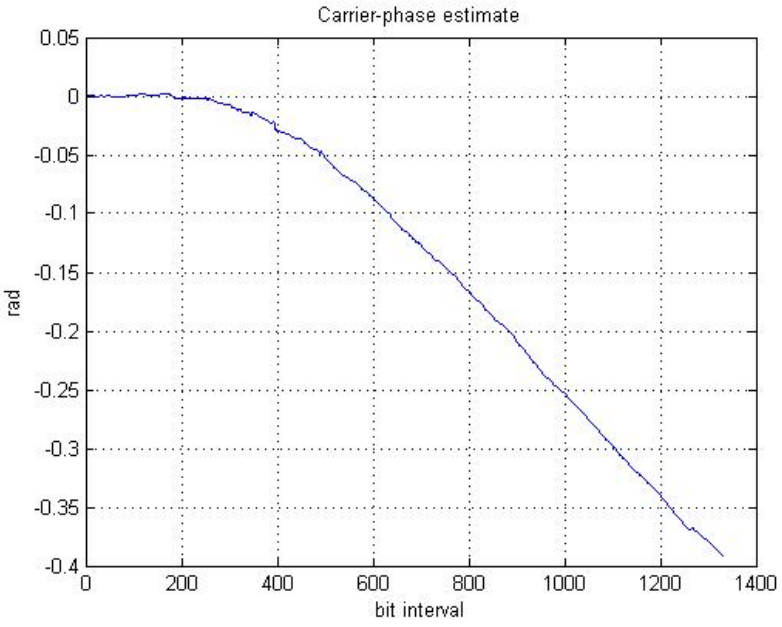

Figure 6.17: Carrier Phase Estimate for Singapore Water 2010

Table 6.6 and Figure 6.18 show the BER result of the equalizers. The UTC method performs better than the other methods when no bit-loading is performed. This is due to smaller number of spectral nulls in the frequency response of UTC TIR. The noise is colored as seen in Fig. 6.19.

Table 6.6: BER performance in Singapore Water 2010

Method	Perfect Feedback	Imperfect Feedback	Imperfect Feedback (Code 1/2 rate)	Bit Loading
OFDM	0.1383	0.1893	0.0983	0.0693
UTC	0.0903	0.1563	0.0692	0.0231
UEC	0.1203	0.1832	0.1102	0.0754
MSSNR	0.1128	0.1692	0.0927	0.0532
Min ISI	0.1128	0.1692	0.0816	0.0183
FD DFE	0.1093	0.1602	0.0826	0.0442
Bit Rate (kbits/s)	4.85	4.85	2.42	2.24

The results in the first three columns of Table IV are documented under the same setting as the first three columns of Table II. In order to showcase the performance of Min ISI, bit loading is performed on the transmit signal. There are 30 sub-carriers with low SNR which are encoded with a convolution code rate of $\frac{1}{3}$. The rest of the sub-carriers are convolution $\frac{1}{2}$ encoded. The BER result of this setting is tabulated in the last column of Table IV. In the case of bit-loading with non-white noise, Min ISI has the lowest BER. Bit loading is able to enhance the performance difference between MSSNR and Min ISI. In Min ISI, high SNR subcarriers perform much better than the subcarriers with low SNR. By loading the high SNR subcarriers with more bits, the overall performance of the system improves. The frequency weighting in Min ISI gives higher priority to high SNR subcarriers in alleviating ISI. Like the GLINT 08 case, UTC is better than UEC due to the nature of their frequency response as shown in figure 6.20.

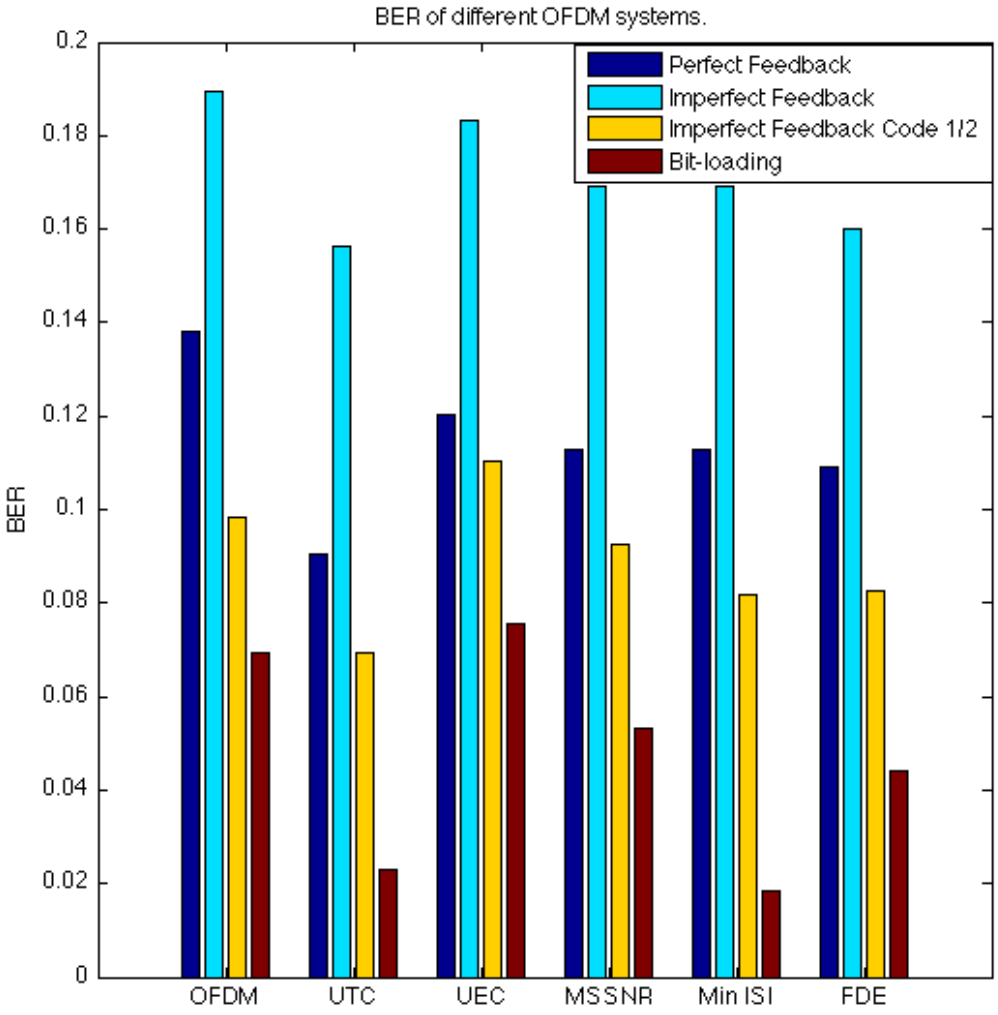

Figure 6.18: BER for Singapore Water 2010

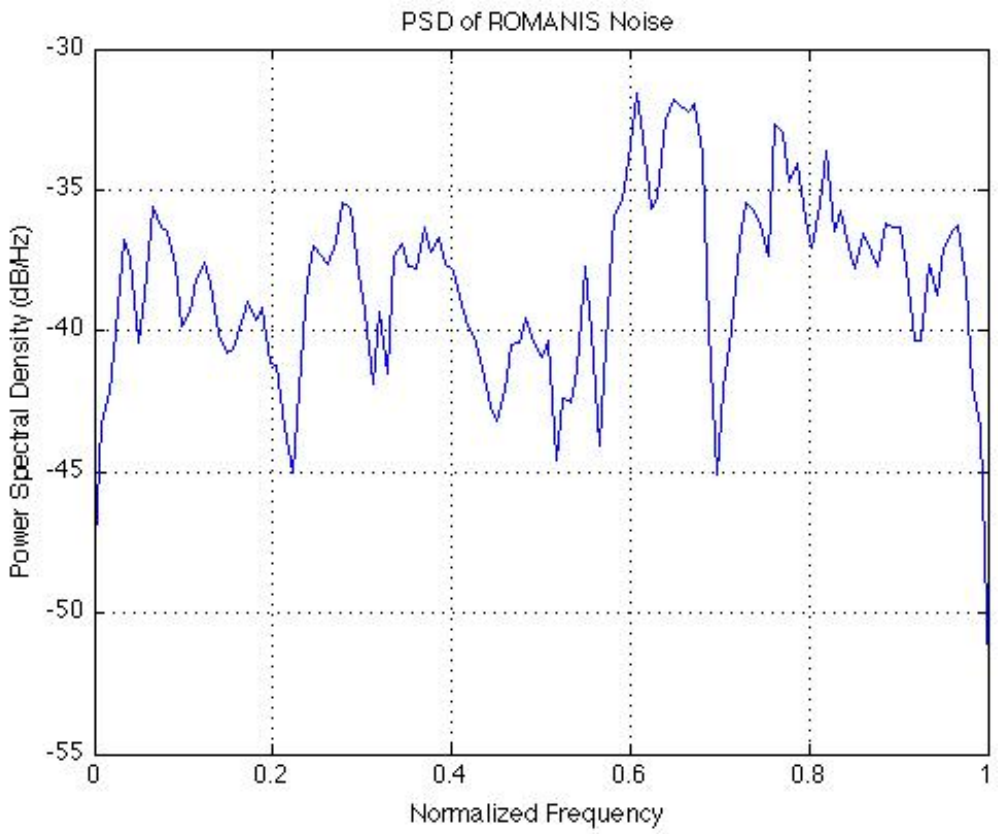

Figure 6.19: PSD of Noise for Singapore Water 2010

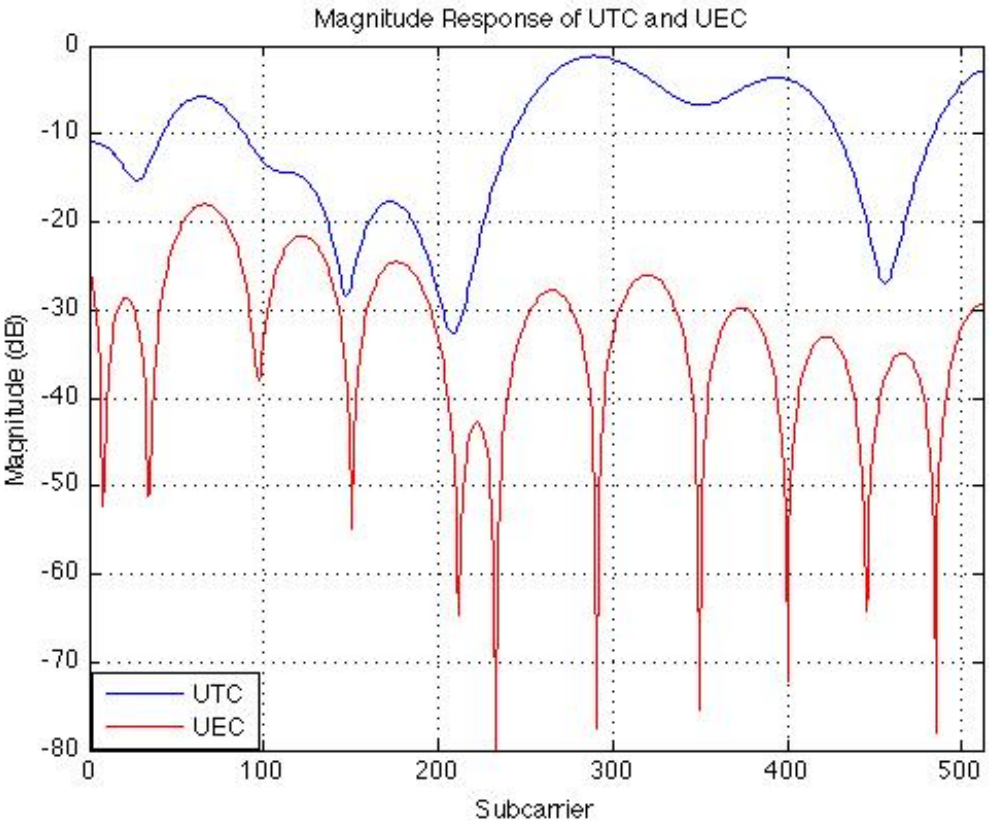

Figure 6.20: Frequency Response of TIR UEC and UTC for Singapore Water 2010

Chapter 7

Conclusion

In an OFDM system with insufficient CP, the ISI and insufficient CP induced ICI is detrimental to effective demodulation. A CSE can shorten the CIR such that the effective impulse response is shorter than the CP, allowing the signal to be orthogonal. For MMSE CSEs, UTC yields better BER results than UEC even though UEC has higher SSNR. This is due to the nature of the UEC frequency response with deep nulls. The Min ISI CSE is a frequency weighted version of MSSNR. When the SNR is different across the sub-carrier, Min ISI CSE performs better than MSSNR. When both the noise and the signal is white, Min ISI reduces to MSSNR. Both time domain CSEs introduce an extra parameter which is the relative delay,. Another alternative to time domain CSEs is the FD-DFE. In the simulation, perfect channel knowledge is assumed. In a real scenario however, the CIR has to be estimated using a pilot sequence. Due to the sparse and long nature of an UWA channel, the natural gradient based channel estimation performs better than the conventional statistical gradient method in terms of convergence speed and steady state error. Having an accurate CIR estimation is

important in ensuring optimal performance of the equalizer. In a non-white noise scenario plus bit loading, UTC and Min ISI perform better than the rest of the equalizers.

7.1 Future Work

Based on simulation and field trial data results, UTC is a recommended choice for UWA channels with large delay spread. However, more work is needed to reduce the complexity of the UTC algorithm while keeping its capability in channel shortening so that it can operate in a real UWA system. The next phase of the research will involve developing a low complexity equalizer. The sparseness of the channel has not been exploited fully in finding the optimal equalizer filters. A lower complexity equalizer can be implemented in a DSP hardware for more practical application of the equalizer. Another potential extension of the current work is a adaptive CSE for OFDM. Previous concern of adaptive CSE is the slow convergence speed due to the length of the CIR. However, we can make use of the IPNLMS or IPAPA algorithm to achieve better result in CSE with less pilots than a conventional LMS equalizer. Lastly, we can explore some other constraint of the time domain MMSE CSE in order to find a more optimal solution to the CSE problem.

References

[1] M. Chitre, S. Shahabudeen, and M. Stojanovic, "Underwater acoustic communications and networking: Recent advances and future challenges," *Marine Technology Society Journal*, vol. 42, no. 1, pp. 103–116, 2008.

[2] M. Stojanovic, "Recent advances in high-speed underwater acoustic communications," *Oceanic Engineering, IEEE Journal of*, vol. 21, no. 2, pp. 125–136, 1996.

[3] M. Chitre, S. Ong, and J. Potter, "Performance of coded ofdm in very shallow water channels and snapping shrimp noise," in *OCEANS, 2005. Proceedings of MTS/IEEE*, pp. 996–1001, IEEE, 2005.

[4] F. Frassati, C. Lafon, P. Laurent, and J. Passerieux, "Experimental assessment of ofdm and dsss modulations for use in littoral waters underwater acoustic communications," in *Oceans 2005-Europe*, vol. 2, pp. 826–831, IEEE, 2005.

[5] M. Stojanovic, J. Catipovic, and J. Proakis, "Adaptive multichannel combining and equalization for underwater acoustic communications," *The Journal of the Acoustical Society of America*, vol. 94, p. 1621, 1993.

[6] M. Stojanovic, L. Freitag, and M. Johnson, "Channel-estimation-based adaptive equalization of underwater acoustic signals," in *OCEANS'99 MTS/IEEE. Riding the Crest into the 21st Century*, vol. 2, pp. 590–595, IEEE, 1999.

[7] M. Lopez, A. Singer, S. Whitney, and G. Edelson, "A dfe coefficient placement algorithm for underwater digital acoustic communications," in *OCEANS'99 MTS/IEEE. Riding the Crest into the 21st Century*, vol. 2, pp. 996–1001, IEEE, 1999.

[8] I. Fevrier, S. Gelfand, and M. Fitz, "Reduced complexity decision feedback equalization for multipath channels with large delay spreads," *Communications, IEEE Transactions on*, vol. 47, no. 6, pp. 927–937, 1999.

[9] E. Sozer, J. Proakis, and F. Blackmon, "Iterative equalization and decoding techniques for shallow water acoustic channels," in *OCEANS, 2001. MTS/IEEE Conference and Exhibition*, vol. 4, pp. 2201–2208, IEEE, 2001.

[10] S. Qureshi and E. Newhall, "Adaptive receiver for data transmission over time-dispersive channels," *Information Theory, IEEE Transactions on*, vol. 19, no. 4, pp. 448–457, 1973.

[11] D. Falconer and F. Magee, "Adaptive channel memory truncation for maximum likelihood sequence estimation," *Bell Syst. Tech. J*, vol. 52, no. 9, pp. 1541–1562, 1973.

[12] N. Al-Dhahir and J. Cioffi, "Efficiently computed reduced-parameter input-aided mmse equalizers for ml detection: A unified approach," *Information Theory, IEEE Transactions on*, vol. 42, no. 3, pp. 903–915, 1996.

[13] J. Chow and J. Cioffi, "A cost-effective maximum likelihood receiver for multicarrier systems," in *Communications, 1992. ICC'92, Conference record, SUPERCOMM/ICC'92, Discovering a New World of Communications., IEEE International Conference on*, pp. 948–952, IEEE, 1992.

[14] J. Chow, J. Tu, and J. Cioffi, "A discrete multitone transceiver system for hdsl applications," *Selected Areas in Communications, IEEE Journal on*, vol. 9, no. 6, pp. 895–908, 1991.

[15] P. Melsa, R. Younce, and C. Rohrs, "Impulse response shortening for discrete multitone transceivers," *Communications, IEEE Transactions on*, vol. 44, no. 12, pp. 1662–1672, 1996.

[16] C. Yin and G. Yue, "Optimal impulse response shortening for discrete multitone transceivers," *Electronics Letters*, vol. 34, no. 1, pp. 35–36, 1998.

[17] D. Daly, C. Heneghan, and A. Fagan, "Minimum mean-squared error impulse response shortening for discrete multitone transceivers," *Signal Processing, IEEE Transactions on*, vol. 52, no. 1, pp. 301–306, 2004.

[18] G. Arslan, B. Evans, and S. Kiaei, "Equalization for discrete multitone transceivers to maximize bit rate," *Signal Processing, IEEE Transactions on*, vol. 49, no. 12, pp. 3123–3135, 2001.

[19] G. Arslan, G. Arslan, B. Evans, R. Baldick, A. Bovik, J. Ghosh, S. Kiaei, and E. Powers, "Equalization for discrete multitone transceivers," 2000.

[20] N. Al-Dhahir and J. Cioffi, "Optimum finite-length equalization for multi-

carrier transceivers," *Communications, IEEE Transactions on*, vol. 44, no. 1, pp. 56–64, 1996.

[21] S. Husain, J. Yuan, and J. Zhang, "Channel shortening through bit error rate minimization for uwb systems," in *Communications Theory Workshop, 2008. AusCTW 2008. Australian*, pp. 130–134, IEEE, 2008.

[22] I. Chen and W. Chin, "Channel spectral flattening in time domain equalizer design for ofdm systems," in *Communications, 2009. ICC'09. IEEE International Conference on*, pp. 1–5, IEEE, 2009.

[23] J. Zhang, W. Ser, and J. Zhu, "Effective optimisation method for channel shortening in ofdm systems," in *Communications, IEE Proceedings-*, vol. 150, pp. 85–90, IET, 2003.

[24] L. Meng, J. Li, A. Huang, J. Song, and H. Zhang, "Mmse channel shortening equalization for ofdm systems with unequal subcarrier powers," in *Communications and Networking in China, 2008. ChinaCom 2008. Third International Conference on*, pp. 1013–1017, IEEE.

[25] A. Song and M. Badiey, "Generalized equalization for underwater acoustic communications," in *OCEANS, 2005. Proceedings of MTS/IEEE*, pp. 1522–1527, IEEE, 2005.

[26] D. Falconer, S. Ariyavisitakul, A. Benyamin-Seeyar, and B. Eidson, "Frequency domain equalization for single-carrier broadband wireless systems," *Communications Magazine, IEEE*, vol. 40, no. 4, pp. 58–66, 2002.

[27] L. Yang and S. Cheng, "Interference cancellation with DFE in frequency

domain for OFDM systems with insufficient CP," *IEICE transactions on communications*, vol. 88, no. 12, pp. 4616–4624, 2005.

[28] D. Falconer, S. Ariyavisitakul, A. Benyamin-Seeyar, and B. Eidson, "Frequency domain equalization for single-carrier broadband wireless systems," *Communications Magazine, IEEE*, vol. 40, no. 4, pp. 58–66, 2002.

[29] J. Cioffi, "A multicarrier primer," *ANSI T1E1*, vol. 4, pp. 91–157, 1991.

[30] P. Robertson and S. Kaiser, "The effects of doppler spreads in ofdm (a) mobile radio systems," in *Vehicular Technology Conference, 1999. VTC 1999-Fall. IEEE VTS 50th*, vol. 1, pp. 329–333, IEEE, 1999.

[31] M. Stojanovic, "Underwater acoustic communications: Design considerations on the physical layer," in *Wireless on Demand Network Systems and Services, 2008. WONS 2008. Fifth Annual Conference on*, pp. 1–10, IEEE, 2008.

[32] B. Hunt, "A matrix theory proof of the discrete convolution theorem," *Audio and Electroacoustics, IEEE Transactions on*, vol. 19, no. 4, pp. 285–288, 1971.

[33] B. Farhang-Boroujeny, *Adaptive filters: theory and applications*. Wiley, 1999.

[34] S. Haykin, "Adaptive filter theory (ise)," 2003.

[35] G. Golub and C. Van Loan, *Matrix computations*. Johns Hopkins Univ Pr, 1996.

[36] P. Davies, N. Higham, F. Tisseur, M. C. for Computational Mathematics, and U. of Manchester. Department of Mathematics, "Analysis of the cholesky

method with iterative refinement for solving the symmetric definite generalized eigenproblem," *SIAM Journal on Matrix Analysis and Applications*, vol. 23, no. 2, pp. 472–493, 2002.

[37] W. Li and J. Preisig, "Estimation of rapidly time-varying sparse channels," *Oceanic Engineering, IEEE Journal of*, vol. 32, no. 4, pp. 927–939, 2007.

[38] S. Gay and J. Benesty, *Acoustic signal processing for telecommunication.* Springer Netherlands, 2000.

[39] K. Pelekanakis and M. Chitre, "Comparison of sparse adaptive filters for underwater acoustic channel equalization/estimation," in *Proc. IEEE ICCS*, vol. 10, pp. 395–399, 2010.

[40] K. Pelekanakis and M. Chitre, "Natural gradient-based adaptive algorithms for sparse underwater acoustic channel identification," *Underwater Acoustic Measurements: Technologies & Results, Kos island, Greece*, 2011.

[41] M. Stojanovic, J. Catipovic, and J. Proakis, "Phase-coherent digital communications for underwater acoustic channels," *Oceanic Engineering, IEEE Journal of*, vol. 19, no. 1, pp. 100–111, 1994.